An Analysis of Climate Change's Impacts on Future Wind Energy Production in California

by

David M. Rasmussen Jr.

A SENIOR THESIS SUBMITTED IN PARTIAL FULFILLMENT
OF THE REQUIREMENTS FOR THE DEGREE OF

Bachelor of Science
(Atmospheric and Oceanic Sciences)

at the

UNIVERSITY OF WISCONSIN-MADISON

2009

Abstract

A changing climate due to anthropogenic forcings is expected to spatially and temporally alter several meteorological variables across the planet, including winds. The recent surge in the production of and investment in wind-generated electricity is vulnerable to these changes. California has taken a proactive stance in addressing the effects of climate change to its current and future energy industry via Governor Arnold Schwarzenegger's Executive Order S-13-08 that initiates the development of a Climate Adaptation Strategy. However, this document omits the United State's third largest producer of wind-generated electricity: California's wind energy industry.

This study acts to append California's Climate Adaptation Strategy with a scientific analysis of foreseen changes in wind speeds at California's largest wind farms that are resultant from an anthropogenically induced climate change. The primary areas in focus are: Altamont Pass, San Gorgonio Pass, and Tehachapi Pass. This study proposes processes and methods to find these changes by analyzing current and past wind speeds from observed measurements and reanalysis data from the North American Regional Reanalysis (NARR) data set and by analyzing mid-21st century predicted wind speeds of the from the newly available North American Regional Climate Change Assessment Program (NARCCAP) data set. The NARCCAP data set's utilization of dynamically downscaled atmosphere-ocean global climate models by the use of regional climate models is of particular importance due to its high spatial resolution. The NARCCAP data is ran with the SRES A2 forcing. Recent work and methods in the wind energy and climate field of research by Breslow and Sailor, Sailor et al., Segal et al., and Pryor et al. is mentioned and considered. However, new methods are explored to qualitatively and quantitatively assess the spatial and temporal variations of winds between current, past, and future periods.

Acknowledgements

I first would like to send my sincere gratitude to my senior thesis advisor, Professor Tracey Holloway, director of the Center for Sustainability and the Global Environment at the Nelson Institute for Environmental Studies. This research would not have been possible if it wasn't for your willingness to guide me through a project that utilizes both my academic interests in atmospheric science and engineering. Your excitement and knowledge in these areas is surely contagious, as I have since developed an even greater curiosity for this kind of interdisciplinary study. Additionally, somehow, amongst your overbooked schedule, you found time to coach me and push me further for getting exciting and clear research results. I cannot give enough appreciation for all of your essential help in this undertaking.

The advising from Nelson Institute for Environmental Studies Professor, Greg Nemet should be recognized here as well. I would like to thank you again for allowing me to help you in your own wind energy related endeavor. Our collaborative work on historical wind speeds in California inspired me to think about my research more deeply because of your unyielding curiosity.

I would like to acknowledge my other academic mentor of sorts, Dr. Matthew Lazzara at the Antarctic Meteorological Research Center. I am grateful for you allowing and supporting me to pursue this goal all while sacrificing my research contributions and time at the Space Science and Engineering Center. I am humbled to have the opportunity to work with someone so passionate and unselfish.

Helping me along the way in this project are several individuals that should also be mention here: SAGE graduate student Steve Plachinski for your introduction and help with NCL, Wisconsin's State Climatologist Dr. John Young and AOS professor emeritus Dr. Ed Hopkins, for your help on getting observed wind data, Dennis Shea, Mary Haley, and Adam

Phillips at NCAR for your help with NCL scripting, and Dave Allured at CIRES at CU-Boulder for your help with NCL scripting as well.

Last, and most importantly, I would also like to thank my parents for their support in helping me obtain a Bachelor of Science degree from one of the world's finest universities. Words cannot begin to thank you for all your love and encouragement. To you I dedicate this thesis.

Other Acknowledgements

Table of Contents

List of Figures

List of Tables

List of Equations

1. Motivation

On November 11th 2008, Executive Order S-13-08 was signed by California

Governor Arnold Schwarzenegger that initiated the scheduled public release of a

comprehensive report that assessed expected impacts to California resulting from climate

change *(1)*. Now available to the public, this report is known as the California Climate

Adaptation Strategy. The Climate Adaptation Strategy included a portion designated to

climate change's impacts on California's infrastructure. The energy infrastructure was

covered in this section of the report, but, although only briefly mentioned, California's large

and vital wind energy industry was surprisingly omitted. As of the 4th quarter of 2008,

California was home to the nation's third largest installment of wind turbines at 2,517

megawatts (MW), only behind Iowa and Texas *(2)*. In addition, California's wind industry is

a huge business. Even before 1991, the total private investment in the industry had

exceeded over $3.2 billion *(3)*. It is possible that a changing climate will endanger these

costly assets. The Climate Adaptation Strategy even acknowledges, "The impacts of climate

change on infrastructure…will be widespread and costly in human and economic terms" *(4)*.

Knowing how a changing climate in California will impact the winds required to create

electricity will be essential information because of their economic and power generation

relevance.

Three days later after passing Executive Order S-13-08, Governor Arnold

Schwarzenegger issued another Executive Order, S-14-08. This time the goal was to have all

retail sellers of electricity in California produce 33% of their electricity load by way of

renewable means by the year 2020. Being a form of renewable energy, wind generated

electricity is relied upon as a means to meet this goal. However, this will be a formidable

task since wind energy in 2007 made up a lone 2.3% of California's gross power output *(5)*. Nonetheless, within a span of four days, California had a mission to assess predicted impacts on the state from a changing climate as well as a plan to drastically boost the production of renewable energy, including wind generated electricity.

With Executive Order S-14-08 enacted, new wind industry developments are planned to occur in the state of California. These additional future investments could come in the form of entirely new wind farm installations. Yen-Nakafuji *(6)* claims that an estimated wind energy output potential of 4,500 MW exists untapped in southern California alone. It is also expected that current wind resource areas will see "re-powering" in the form of upgrades to existing antiquated technology from the 1980's when wind energy was in its infancy in California. Many of these turbines have power outputs around 150 kilowatts (kW), a full order of magnitude smaller than wind turbines being installed today. Upgrades to these units could greatly increase power production at some of California's prime wind resource areas (6). It is evident that plans are present to meet the ambitions of Executive Order S-14-08.

These planned developments require financial backing. In order to attract confident investors, it must be evident that their support will be profitable over the lifetime of the turbine units. A changing climate is a new variable that should be considered by companies and individuals supporting wind generated electricity. Current wind speeds are relied upon to drive these machines and should not be considered immune to a changing meteorological environment. Therefore, it is crucial for investors to be briefed on the effects of climate change on wind energy.

The climate in California is changing, and the changes are expected to have impacts on the state's current and future infrastructure. In addition, goals have been set by the Governor to drastically increase the production of renewable energy resources, including wind power. Thus, knowing how future climate change will affect California's wind energy investment is dually essential for the future. This paper's intention is to be a potential supplement to the California Climate Adaptation Strategy, and will assess the future of California's wind industry by using and building upon published scientific methodologies used in prior studies on climate change's effect on the well being of wind energy in the future.

1.1 Wind Speed Transformations Due to a Changing Climate

The US surface wind fields are susceptible to transformations with an increase in atmospheric CO_2. General circulation model (GCM) output has shown a decrease in the magnitudes of the north-south temperature gradients. This change could possibly shift the track of mid-latitude weather systems northward and result in changes to the continental winds *(7)*.

Winds are a vulnerable meteorological variable and are consequently hard to predict. Many climatological factors affect wind power resources such as: temperature, topography, precipitation, daytime insolation, and dominant upper atmospheric circulations. Breslow and Sailor *(8)* claim, long-term variability in wind speeds on scales of decades "introduce(s) an element of risk" into the decision process for siting new turbine units. It has also been suggested that the planet's changing climate driven by a carbon dioxide emissions forcing will increase the uncertainty in projecting wind speeds decades into the future. However, methods have been devised to assist in estimating future wind. Specifically, it has been

claimed that the chief factor in determining available wind speeds is using wind speed statistics, such as mean wind speeds, wind speed variance, and wind speed frequencies *(8)*. These tools are often considered when estimating predicted conditions.

The potential changes in wind speeds due to occur over this century are very valuable pieces of information, especially for Californian utility companies operating wind turbines and wind energy investors. This is due to the fact that the general power potential function is directly proportional to the cube of the mean wind speed. Thus, small changes in wind can be greatly amplified when considering electricity generation. This can be seen in Equation 1.1. Where V is the magnitude of the wind going through the rotor (m/s), A is the cross sectional area of the turbine rotor (m^2), and ρ is the density of the ambient atmosphere (kg/m^3) *(8)*.

$$P_{Pot.} = \frac{1}{2}\rho AV^3 \quad \textbf{Equation 1.1}$$

Thus, small changes in future mean wind speeds can consequently have a very large long-term effect on annual power generation. Meaning millions of dollars in profit and production of thousands of MW of electricity over decades could be lost if a wind farm development succumbed to a lessening of wind resources in this century due to a changing climate.

The density of available power (W/m^2) from the wind in a region is directly related to the wind speeds in that same area. The wind industry uses a particular scale for quantifying this power density. Table 1.1 gives the scale for wind power classes based on the wind speeds at both 10 m and 50 m. Each wind power class also has a typical wind power

density range associated with it. This study will use this conversion method frequently to give a clearer indication of the availability of wind power resources from meteorological variables such as wind speed.

Classes of Wind Power Density at 10m and 50 m[a]				
10 meters			50 meters	
Wind Power Class	Wind Power Density (W/m²)	Wind Speed[b] (m/s)	Wind Power Density (W/m²)	Wind Speed[b] (m/s)
1	<100	<4.4	<200	<5.6
2	100-150	4.4-5.1	200-300	5.6-6.4
3	150-200	5.1-5.6	300-400	6.4-7.0
4	200-250	5.6-6.0	400-500	7.0-7.5
5	250-300	6.0-6.4	500-600	7.5-8.0
6	300-400	6.4-7.0	600-800	8.0-8.8
7	>400	>7.0	>800	>8.8

Table 1.1 Wind Power Classes (Renewable Resource Data Center, (9) (a) Vertical extrapolation of wind speed based on the 1/7 power law (b) Mean wind speed is based on the Rayleigh speed distribution of equivalent wind power density. Wind speed is for standard sea-level conditions. To maintain the same power density, speed increases 3%/1000 m (5%/5000 ft) of elevation.

1.2 Planned Methodology

In order to spatially and temporally assess such statistical changes in the wind resources at wind farms in California, three particular regions were chosen to study: Altamont Pass, San Gorgonio Pass, and Tehachapi Pass. These particular regions encompassed almost 90% of California's total wind energy output in 2003 and they contributed around 10,877 of California's 11,655 wind turbine units *(6)*. At these locations there exists wind turbines that make up numerous wind farms erected by several different investors. For simplicity, in this paper these multiple wind farms in the three areas of focus will be collectively referred to as their location's name, such as the Altamont Pass wind farm, even though there exists more than one wind farm at the geographical location of Altamont Pass.

At the previously mentioned locations, the present and historical winds and the predicted future winds will be both qualitatively and quantitatively assessed for spatial and temporal changes occurring in a changing Californian climate due to an anthropogenically induced GHG forcing. In order to separate the natural variability in wind speeds from the variability associated with climate change, the present and historical wind speed cycles will be subtracted from the predicted climatic record to manifest the important climate change induced variations. This method has been explored and applied to the global wind industry by Breslow and Sailor *(8)* and Segal et al. *(10)*, and more recently, Prior et al. *(11, 12)* and Sailor et al *(13)*. In this paper, the natural wind speeds will be produced from both observed measurements from the National Climatic Data Center (NCDC) and reanalysis data from the North American Regional Reanalysis (NARR) dataset from the National Center for Environmental Prediction (NCEP). The future climate record wind speeds from the mid 21st century will be extracted from recently released datasets from the North American Regional Climate Change Assessment Program (NARRCAP) from the University Cooperation for Atmospheric Research (UCAR). With these datasets, valuable insight on the deviations from future and current conditions will be revealed.

2. Current and Past Winds in California

In order to assess future wind speeds at the location of the three wind farms focused on in this paper, the current and past wind speeds at the sites must be considered. Without knowing what current spatial and temporal wind energy production exists in California, the outlook of future power generation cannot be properly assessed. Also required to be understood before viewing the future projections are the meteorological and climatic characteristics that generate the winds at the wind farms, discussion of the current and past

wind speed datasets, methods of extrapolating wind speeds to turbine hub heights, and viewing current and past wind speeds both spatially and temporally.

2.1 Wind mechanisms at the wind farms sites

The dominant meteorological forcings that create the winds over the state are important for assessing larger scale changes. The high air pressure that resides in the northeast Pacific Ocean primarily runs the climate and circulation in California. This air mass drives the prevailing westerly winds during the majority of the year, but the local topography on shore usually interrupts this dominant flow and redirects the wind. In the winter, this dominant circulation is modified somewhat by migrating centers of pressure, thus consequently altering the speed and direction of California's typical winds. For instance, over the Great Basin, to California's east, a persistent region of high pressure is present, and on the Californian coast, frequent low pressure disturbances advance from the Pacific. These converging air masses drive a strong easterly pressure gradient wind flow throughout much of the state, particularly at higher elevations *(14)*.

The thermal gradient that exists between the some 2,150 km of coastline and the vast interior of the state functions as the typical driver in the high wind speeds in the areas of the Californian wind farms. Cool air strips off of the surface of the Pacific Ocean and is then forcefully squeezed through the few breaks in the coastal mountain ranges that act as gateways to California's inland regions of warm dry air. These passes, or wind corridors, as they are often called, include Altamont Pass in central California and San Gorgonio Pass and Tehachapi Pass in Southern California. The break in the mountains at San Francisco Bay is an example of where, on most warm summer days, a "sea breeze" will move cool air from San Francisco Bay through the Oakland hills and in to California's Central Valley *(15)*. The

heat from the Sun in the Central Valley then energizes and lifts the air over the hills around Livermore and into "channels" that bring the air to Altamont Pass, thus fueling the wind farms. These "channels" are around 14 kilometers in length and lie in the western edge of the Central Valley. The air that moves through these passages is known to have its movements accelerated when an inversion layer is present *(16)*. Another example of this terrain feature can be viewed in Figure 2.1 where the 1 km wide San Gorgonio Pass can be seen with Interstate 10 running along its basin *(17)*. The thermal gradient along California's coast is essential to the wind farms at these mentioned locations.

Tehachapi Pass is sometimes considered a desert wind corridor as it lies in an area of particularly high aridity. Winds there are typically channeled south, down through the San Joaquin Valley, to the Mojave Desert, producing optimal resources for the Tehachapi wind farm. In addition, some of the Tehachapi wind turbines that are perched atop the Tehachapi Mountains are, from time to time, able to tap into strong upper air winds. This is possible since they are placed at such high elevations, some around 1200 meters. These particular turbines and their placement locations can be seen in Figure 2.2.

Another event at work that creates unusually high winds at Tehachapi is the unequal heating of air basins separated by the Tehachapi Mountain range. This particular process creates an additional wind flow over the range between the two air masses with different temperatures. This process can sometimes create wind speeds faster than those of upper level winds *(15)*.
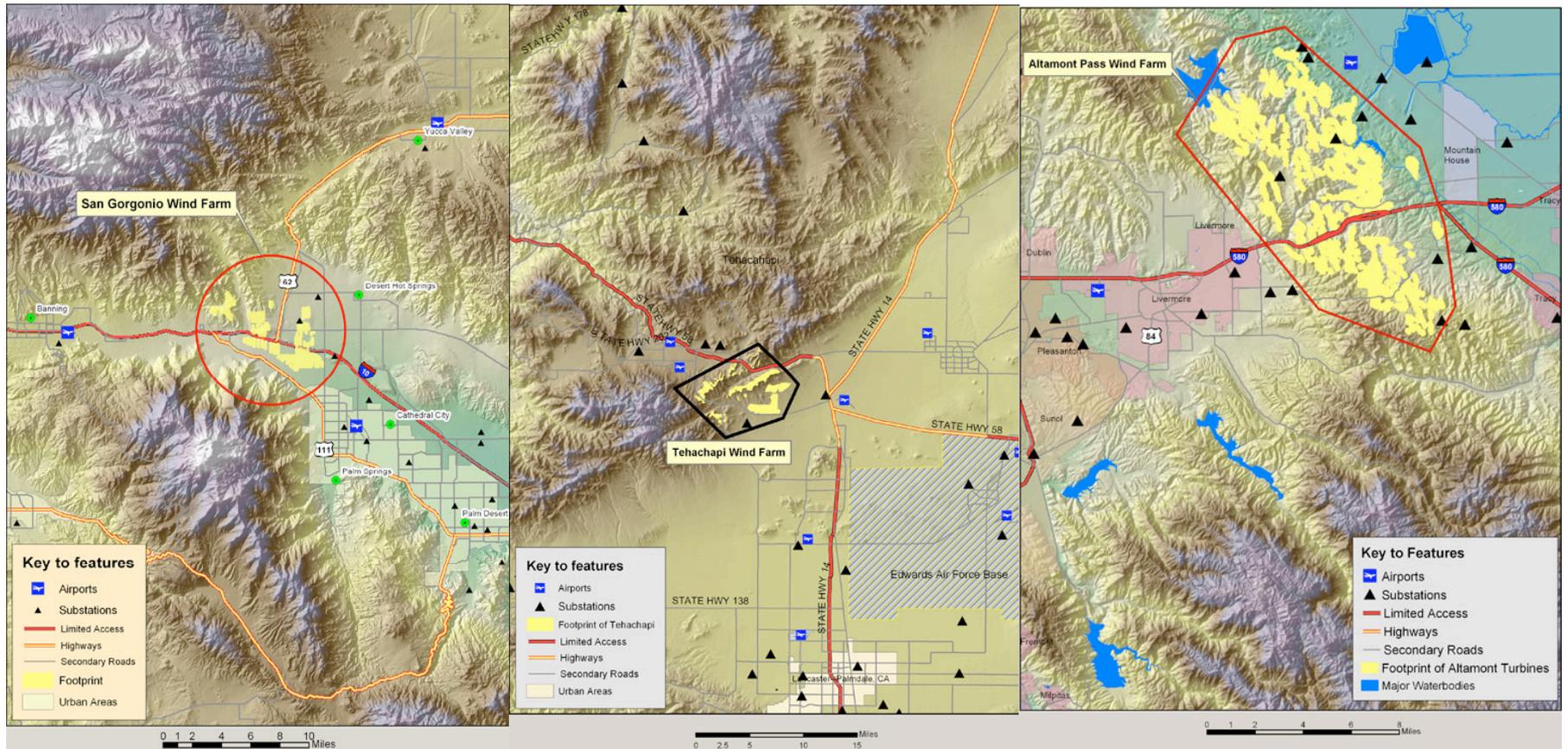
Figures 2.1, 2.2 and 2.3 are topographic and civil maps showing the region around San Gorgonio, Tehachapi, and Altamont Passes, respectively. (18)

Tehachapi Pass and the rest of these passes are some of the windiest areas in California and in the contiguous United States. They all have an annual average wind power class of 6 out of a possible 7, with winds annually averaging around 7 m/s at the surface *(15)*. Table 2.5 lists the possible wind power class categories.

2.2 Extracting Winds from NARR Data

The North American Regional Reanalysis (NARR) data in this project was used for gathering the historical winds at the wind farm locations for the period of 1979 – 2008. Breslow and Sailor *(8)* chose to utilize the 0.5-degree gridded historical data set known as VEMAP that had data from 1948-1978. Pryor et al. *(11)* chose to utilize the NCEP/NCAR 1.875 degree reanalysis data from 1961-1990. Neither author have had the opportunity to use the NARR data set, as the NARR project is a fairly recent undertaking as it was completed in 2004. It is based off the NCEP Eta model and its corresponding 3D-Var Data Assimilation System (EDAS). The resolution is 32 km in the horizontal and is comprised of 45 discrete vertical layers, the same as the Eta model prior to 2000. The high resolution of this reanalysis data and the number of variables extractable makes it unique from other data sets. The NARR data that was used incorporates most of the observations from the updated Global Reanalysis, version GR2. The only satellite data that was used in the NARR project was from NESDIS for temperature and precipitable water over the oceans within the NARR grid domain and it was also used for vegetation parameterizations *(19)*.

The NARR data were downloaded from the providers at the National Centers for Environmental Prediction (NCEP) and the National Center for Atmospheric Research (NCAR), and was obtained in the form of monthly means. Each NARR file included both u and v components of the wind averaged for one month.

2.3 Viewing the data with NCAR Command Language (NCL)

NCAR Command Language, or commonly known as NCL, is Fortran based program. NCL is a free interpretive language that was designed for the purpose of scientific data processing and visualization. It was developed at the Computational & Information Systems Laboratory (CISL) at the National Center for Atmospheric Research (NCAR). Almost all of the maps and data analysis in this paper have been created with the use of NCL *(20)*.

2.4 The NARR Grid

NCL was used to extract the winds from the NARR data at the wind farm locations. A script took an input of the wind farm latitude and longitude coordinates and then outputs a corresponding NARR grid point nearest to the inputted location. A separate NCL script was then utilized to output the wind magnitude from the u and v components at the specified NARR grid point and pressure level in the form of an ASCII text file. The ASCII text file could then be imported to a number of different programs for data analysis and plot creations. Table 2.1 lists the numerical grid point coordinates of the wind farms on the NARR grid.

Wind Farm	NARR Grid Box Location
Altamont	104, 132
San Gorgonio	86, 145
Tehachapi	93, 141

Table 2.1 NARR grid box locations for the wind farms

The map of California, Figure 2.4, overlaid with the NARR 221 grid indicates the exact location of the wind farms within their corresponding grid boxes *(19)*. Notice on Figure 2.4 that some of the wind farms fall on or near the grid cell borders. For instance, it

appears that the Tehachapi wind farm lies in the middle of four different grid cells. This

visual appearance may be due to the size of the markers on the plot itself, but, nonetheless,

the adjacent grid cells were checked for data values that were closest to being inline with the

observed winds measured for that particular wind farm.
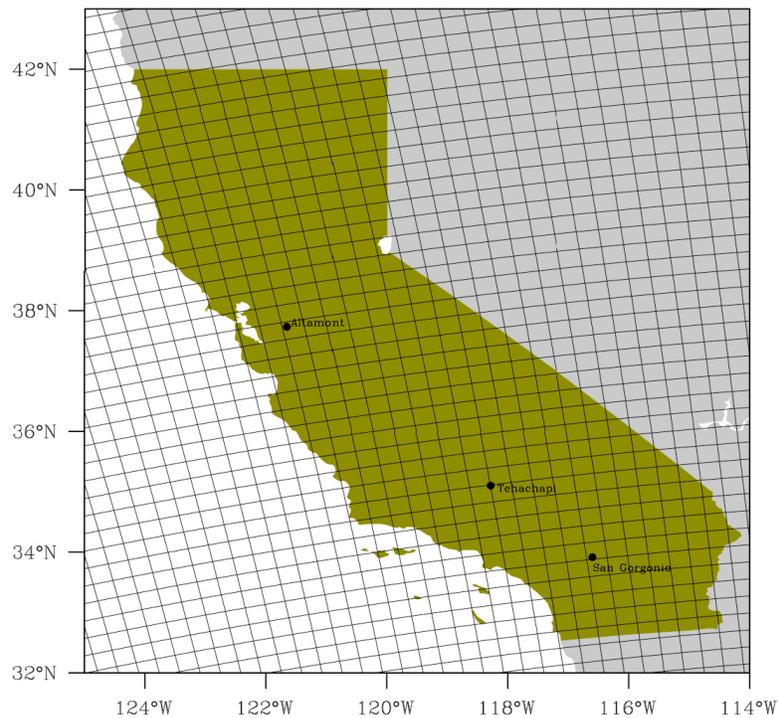
***Figure 2.4 The NARR resolution over the state of California showing the NARR grid cells and the actual latitude and longitude
coordinate locations of the wind farms in their corresponding grid cells***

    The numerical assimilation techniques used with the NARR data set are made

possible by substituting finite difference approximations for spatial derivatives. The NARR

grid-point array, at any level, has its grid points made up of various indices, such as *(i, j),*

indicating their position in the grid. All calculations for the NARR data set are done

exclusively at the grid points themselves. Every point not on the boundaries on a square one

dimensional grid are made up of a five point stencil pattern which includes the point itself

and its four "neighboring" points, which are used to calculate derivatives at the point where the neighboring points surround. This structure can be seen in Figure 2.5.
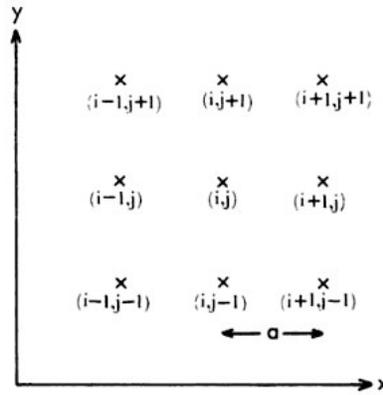
Figure 2.5 A visual representation of the modeling grid (20)

The distance between the grid points, known as the grid length, is 32 km for the NARR data set. In the equation below, an example derivative, $\partial u/\partial x$, at the grid point (i, j) is given by Equation 2.1, where d is the distance between grid points *(21)*. From basic knowledge of calculus and derivatives, it can be said that Equation 2.1 is averaging the data that is inside the grid boxes *(22)*.

$$\left(\frac{\partial u}{\partial x}\right)_{i,j} = \frac{u_{i+1,j} - u_{i-1,j}}{2d} \text{ Equation 2.1}$$

2.5 Converting Between Geometric and Isobaric Heights

The NARR wind data has to be extracted at distinct pressure levels, not elevations, due to they way the data is assimilated. To account for the various heights of the wind farms above sea level, the geometric heights of the wind farms had to be converted to isobaric pressure levels or geopotential heights. Doing this allows for both u and v components of the wind to be extracted from the multiple possible isobaric pressure levels that exist in the NARR data. All in all, there are 29 distinct pressure levels in the NARR data set ranging from 1000 mb at the surface to 100 mb at the upper limit of the troposphere *(23)*.

In an assumed vertically isothermal atmosphere, the pressure at some given elevation can be calculated. Equation 2.2, derived from the hydrostatic equation and the ideal gas law, allows for the needed conversion between geometric and isobaric height. The equation mathematically says that pressure decreases exponentially with elevation *(24)*.

$$p(z) = p_0 \exp\left(\frac{z}{H}\right) \ \ where \ H = \frac{R\overline{T}}{g}$$

Equation 2.2

Solved for p, the pressure at the wind farm location (Pa), and using p_0 as a reference pressure at sea level (Pa), 1.013 x 10^5 Pa, or 1013 mb, Equation 2.2 can give the approximate equivalent pressure for an elevation at some height above sea level (m), z. H is the scale height, a constant. Both gravity and column-averaged temperature were held constant, and the column-averaged temperature was assumed to be 20° C or 68° F, a fair approximation of a yearly mean temperature for the three Californian wind farms used in this study. The calculated equivalent pressures are listed in Table 2.2 along with the nearest extractable NARR pressure levels, and the corresponding approximate elevations of the wind farms.

Wind Farm	Elevation (m)	Calculated Equivalent Pressure (mb)	Nearest NARR Equivalent Pressure (mb)
Altamont	~320	976	975
San Gorgonio	485	957	950
Tehachapi	~1160	885	875

Table 2.2 Elevations and equivalent pressure levels for the wind farms. Elevations from the United States Geological Survey

Figure 2.6 illustrates the process of extracting the winds at the surface from NARR isobaric levels. As shown, the winds at the wind farm at an elevation of 425 m in the schematic would be extracted from the 950 mb level, as it is the nearest level in the NARR data set that is closest to the calculated surface pressure. The 975 mb level would not be a

possible choice as it lies below ground level at the wind farm site. It is assumed that the elevations of the base of the observations sites lie roughly at the same elevation of the base of the turbines at the wind farms themselves, except for Altamont Pass, where a large change in elevation from the observation site and the wind farm exists. This can be seen in Figure 2.3.
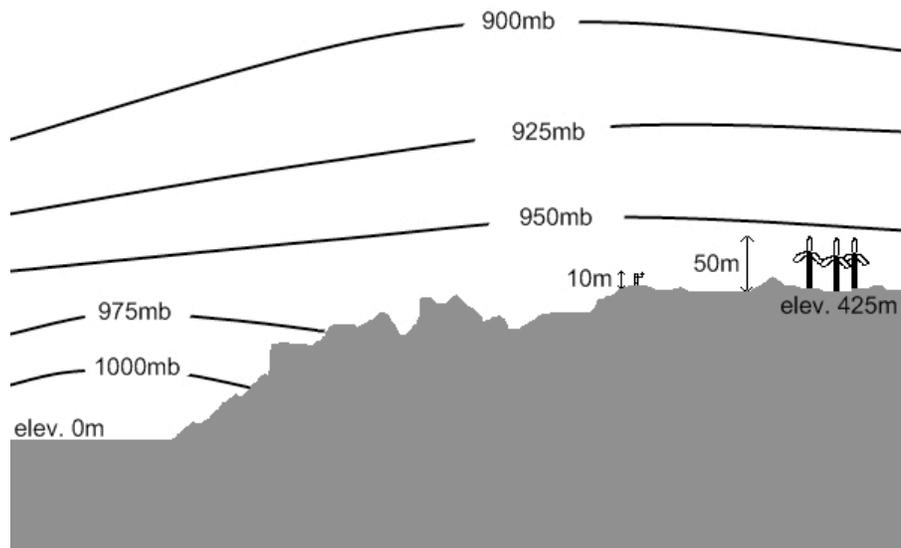
Figure 2.6 Schematic visually showing the method for NARR wind extraction from isobaric pressure levels to accommodate for the presence of elevations deviating from sea level

2.6 Using Available Observed Wind Speed Data

In verifying the effectiveness of the NARR wind data, wind observations from locations near the wind farms were used. The source of the wind data was from automated surface observing systems (ASOS) at airports and remote automated weather stations (RAWS) used for the purpose of fire danger and air pollution monitoring. The source of the ASOS data was the National Climatic Data Center (NCDC). The Western Regional Climate Center (WRCC) was the source for the RAWS measurement. After it was obtained, the data was converted to monthly means and then to quarterly means from its original form of hourly and daily means in an effort to smooth time series plots created for this paper. It

should be mention that by doing this, some variability on smaller time scales is lost. However, this study is focused on longer temporal scales such as interannual and annual variability, and so such smoothing processes are not a substantial issue. Table 2.3 and 2.4 lists the latitude and longitude that the observations were taken from for each wind farm as well as the latitude and longitude coordinates for each wind farm to get an idea how close or far they are to one another.

Wind Farm	Coordinates
Altamont Pass	37.732°N -121.652°E
San Gorgonio	33.916°N -116.600°E
Tehachapi	35.102°N -118.282°E

Table 2.3 Wind Farm Coordinates (24)

Observation Site	Coordinates
Livermore Municipal Airport (ASOS)	37.700°N -121.816°E
Palm Springs International Airport (ASOS)	33.830°N -116.500°E
Jawbone, CA (RAWS)	35.280°N -118.216° E

Table 2.4 Observation Site Coordinates from USGS and the WRCC

2.7 Extrapolation of Winds to Turbine Hub Heights

The stability of the atmosphere at the locations of the wind farms should be assessed before extrapolating surface wind speeds to the turbine hub heights to improve accuracy in the calculations. Since its inception, the Pasquill stability method has been the most commonly used method in evaluating the quantity of atmospheric turbulence present for given conditions of wind speed and daytime solar insolation. Most popular with atmospheric pollution dispersion, the Pasquill stability index is defined as a series of classes from A to F, where A is highly unstable and F is highly stable *(26)*. Assuming strong daytime insolation and an average surface wind speed in the realm of 3-5 m/s at the wind farm locations, by Pasquill *(26)* the corresponding atmospheric stability should be classified as moderately unstable, or stability class B.

Because vertical shear exists in the wind from the ground level to the heights of the turbine hubs due to surface friction, the winds at the hubs need to be correspondingly amplified *(27)*. This is typically done with two methods: the one-seventh-power law method and the logarithmic wind profile method. Both methods assume a neutrally buoyant atmosphere or surface layer. However, where the three wind farms in this paper are located, there normally exists an unstable atmosphere during the daytime hours, as established previously by the Pasquill index and the previously mentioned atmospheric conditions. This fact must be considered, as an atmosphere's winds will be affected by both the mechanical and convective turbulence present. Elliott *(28)* also found that the $1/7^{th}$ power law yields more accurate estimates for wind speeds aloft in open flat areas with small roughness lengths. This is not the case for the California wind farms under study. Thus, this paper utilizes the logarithmic wind profile equation with a modification that adds a so-called Monin-Obukov parameter to account for the atmospheric instability, similar to Pryor et al. *(8)*. Equation 2.3 gives the Monin-Obukov length for a moderately unstable atmosphere, Pasquill stability class B *(29)*.

$$\frac{1}{L} = -.037 + .029 \log_{10}(z_0) \quad \text{Equation 2.3}$$

The roughness parameter, z_0, in Equation 2.3 corresponds to hilly or mountainous terrain at the wind farm locations and observation sites. Observations from Palm Springs International Airport and Livermore Municipal Airport use a roughness parameter that is typical of an urban area. Equation 2.4 gives the logarithmic wind profile equation with the addition of a parameter for a turbulent surface layer *(30)*.

$$\frac{\bar{u}}{u^*} = \left(\frac{1}{\kappa}\right)\left[\ln\left(\frac{z}{z_0}\right) + \Psi\left(\frac{z}{L}\right)\right] \quad \text{Equation 2.4}$$

In Equation 2.4, $\bar{u}$ is the mean wind speed at height z, u_* is the friction shear

velocity, κ is the von Karman constant, determined to be .35, z_0 is the previously mentioned

surface roughness parameter, and $\Psi\left(\dfrac{z}{L}\right)$ is the stability parameter adjustment to the

logarithmic wind profile equation.

Equation 2.6 is the stability parameter for unstable conditions $\left(\dfrac{z}{L} < 0\right)$ and is given by

Paulson *(31)*. It includes the following Businger-Dyer relationship, Equation 2.5, determined

empirically by, Businger, et al. *(32)* and Dyer *(33)*.

$$\phi_M = \left[1 - \left(\frac{15z}{L}\right)\right]^{-1/4} \text{ For } \left(\frac{z}{L} < 0\right) \quad \text{Equation 2.5}$$

$$\Psi_M\left(\frac{z}{L}\right) = -2\ln\left[\frac{(1+\phi_M)}{2}\right] - \ln\left[\frac{\left(1+\phi_M^2\right)}{2}\right] + 2\tan^{-1}(\phi_M) - \frac{\pi}{2} \quad \text{Equation 2.6}$$

To interpolate mean wind speeds, $\bar{u}_1$, to a geometric height, z_2, from a geometric

height, z_1, Equation 2.7 was derived. In Equation 2.7, z_2 corresponds to the turbine hub

height, and z_1 is the height of the measurement tower. Equation 2.7 is also given by Pryor et

al. *(11)*.

$$\bar{u}_2 = \bar{u}_1 \frac{\left[\ln\left(\frac{z_2}{z_0}\right) + \Psi_M\left(\frac{z}{L}\right)\right]}{\left[\ln\left(\frac{z_1}{z_0}\right) + \Psi_M\left(\frac{z}{L}\right)\right]} \quad \text{Equation 2.7}$$

The wind speeds in the wind speed time series plots in this paper are all computed

with equation 2.7 and extrapolated to 50 m, as they are in NREL *(34)*. However, the wind

speeds in the wind speed contour maps in this paper are not extrapolated and are all at 10 m,

as they are in Breslow and Sailor *(8)*.

There is an amount of error that needs to be considered when extrapolating winds from the surface to a specified height above ground. According to the National Renewable Energy Lab's (NREL) wind resource assessment project conducted in the early 1980's, at 38 sites where winds were measured to be power class 3 or greater at 50 m, only 42% of the sites would have the same power if their 10 m wind speeds were extrapolated to 50 m with the one-seventh-power law equation that assumes neutral stability. Equation 2.8 is the one-seventh-power law equation *(35)*.

$$\frac{V_1}{V_0} = \left(\frac{Z_1}{Z_0}\right)^{\frac{1}{7}} \textbf{Equation 2.8}$$

In fact, 37% of the sites had wind speeds that exceeded the initial wind speed estimate given by the equation, and half of the 37% has actual wind speeds that exceeded the estimates by two or more power classes. However, in areas of ridge crests, hilltops, and other terrain features that amplify the winds, 21% of the 38 sites in these areas reported that actual 50 m measured wind speeds were considerably less than they were estimated to be by using extrapolation methods on 10 m winds.

Almost all the wind turbines in this paper are located in such regions where terrain features accelerate the wind, so according to NREL's early 1980 study, it is likely that the extrapolated wind speeds may be over estimates *(36)*. Nonetheless, it has to be considered that methods of extrapolating wind speeds with such an equation that assumes an unstable atmosphere, like Equation 2.7, will resolve more realistic wind speeds.

2.8 Interannual Temporal Variability for California's Wind Farms

Figure 2.7 is a time series for quarterly averaged wind speeds, in meters per second, extrapolated to a 50 m turbine hub height at the Tehachapi wind farm location. Quarterly

means were chosen in an effort to smooth the time series and see more clear interannual variability. The time series runs from the beginning of 1992 to the end of 2008. The range of wind speeds on this graph is approximately between 2 and 8 m/s with the highest wind speeds occurring in the second quarter of each year, or in the months of April, May, and June. The NARR and observed data correlates well together on a year-to-year basis with annual variability in speeds being easily identifiable. However, the wind speeds do correlate better during the times of the windier months than they do during the times of the year when the wind is not as strong. The overall correlation between the NARR and observed data sets is .93, the best out of the three data sets for the three wind farms.

There also appears to be a slight decrease in year-to-year variability between 1998 and 1999, possibly a signature of the strong 1998 El Niño Southern Oscillation (ENSO) event *(37)*.

It should be noted that the observed winds used to compare those from the NARR data files at the Tehachapi wind farm were not extrapolated. This is due to the fact the majority of the wind farm's turbine hubs are approximately at the elevation of the observations. Some may be placed at even higher elevations due to the mountainous terrain in the vicinity of the Tehachapi site. Looking at the time series in Figure 2.7, it appears that this was the appropriate method to account for the elevation of the wind observations as the observed data follows the NARR well. The NARR winds were still extracted at the same nearest pressure level as the observations for Tehachapi. The variation in turbine siting proves that these time series are only a rough approximation intended to give insight into the year-to-year variability.
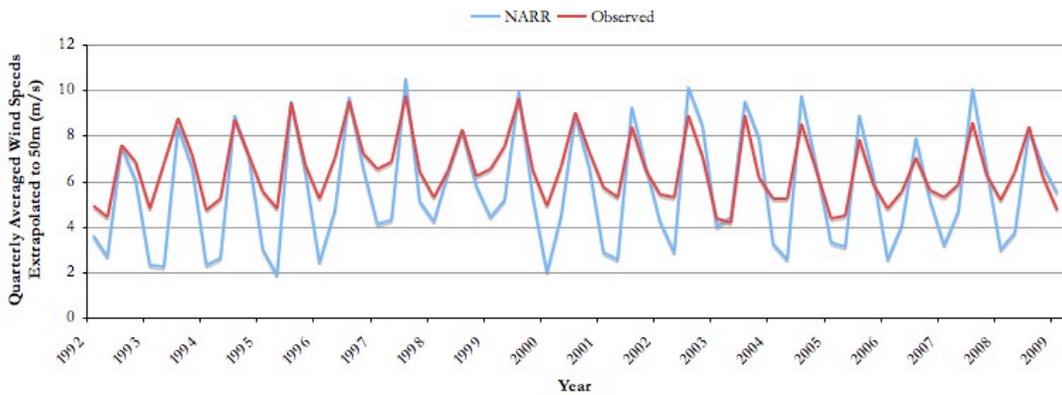
Figure 2.8 is a time series for quarterly averaged wind speeds, in meters per second, extrapolated to a 50 m height for the Altamont Pass wind farm location. The time series runs from the beginning of 1979 to the end of 1999. The observed data is from the Livermore Municipal Airport just west of Livermore, CA adjacent to Interstate 580. *See Figure 2.3* The observed data measurements are approximately 4 km west from the perimeter of the wind farm itself.

Figure 2.7 Time series for Tehachapi Pass with quarterly averaged wind speeds (m/s) extrapolated to 50 meters from 1992 to 2009. Created with NARR and observed wind data. Note: Observed wind speeds are not extrapolated because measurements are from some of the heights of the turbine hubs. Observed wind speed annual range was chosen because data was only available from 1992 to present.
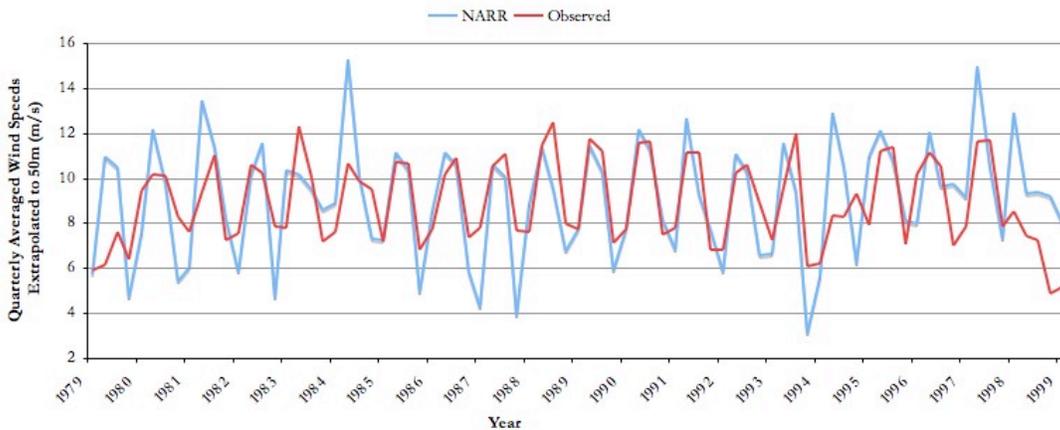
Figure 2.8

Figure 2.8 Time series for Altamont Pass with quarterly averaged wind speeds (m/s) extrapolated to 50 meters from 1979 to 1999. Created with NARR and observed wind data. Note: The observed wind speed annual range was chosen because data was only available to the end of 1998.

21

From Figure 2.3, it can also been seen that the wind farm and the observation site are not at the same elevation. Many of the turbines are located on elevated ridgelines some 170 m higher than the elevation of the observed data from the Livermore Municipal Airport *(18)*. Correspondingly, the extrapolation of the observed winds at the airport must be raised more than usual to accommodate for the dramatic elevation difference between the wind farm and the airport. As a result, there are more discrepancies in the magnitudes wind speeds than the other data sets. A greater height of extrapolation is subject to a greater amount of uncertainty.

The approximate range of wind speeds on this graph is between 6 and 12 m/s with the highest wind speeds from the NARR data set usually occurring in the second quarter of each year. It can be seen, however, that in some stretches of years, such as from approximately 1985 to 1992, that there are two, almost equivalent, windy quarters occurring in succession with one another. Visually this can be seen with the peaks of wind speed having "flat tops", as compared to "pointy" peaks where a particular quarter exclusively has the highest wind speeds for that year.

Nonetheless, the wind speeds correlate better during windier months than they do during the times of the year when the wind is not as strong. In the time series plot, the annual variability in the observed wind speeds does not correlate well with the NARR data set for the first three years plotted. Periods of high wind speeds in the first three years are not as well aligned as they were for the data sets for Tehachapi Pass. However, between 1985 and 1992, the annual variability for the NARR and observed winds are better correlated with periods of high and low wind speeds matching up better than previous years in the time

series for Altamont Pass. The overall correlation between the NARR and observed data sets is .58, the least correlated between the three wind farms.

The also appears to be a slight decrease in year-to-year variability between 1994 and 1995, as well as between 1998 and 1999. These are possibly signatures of the moderate 1994 ENSO event and the strong 1998 ENSO event *(37)*.

Figure 2.9 Time series for San Gorgonio Pass with quarterly averaged wind speeds (m/s) extrapolated to 50 meters for a 20-year period from the beginning of 1979 to the end of 1998. Created with NARR and observed wind data. Note: The observed wind speed annual range was chosen because the wind speed data available after 1998 was deemed erroneous. Wind speed data for 1996 was unavailable, as seen in the time series plot.
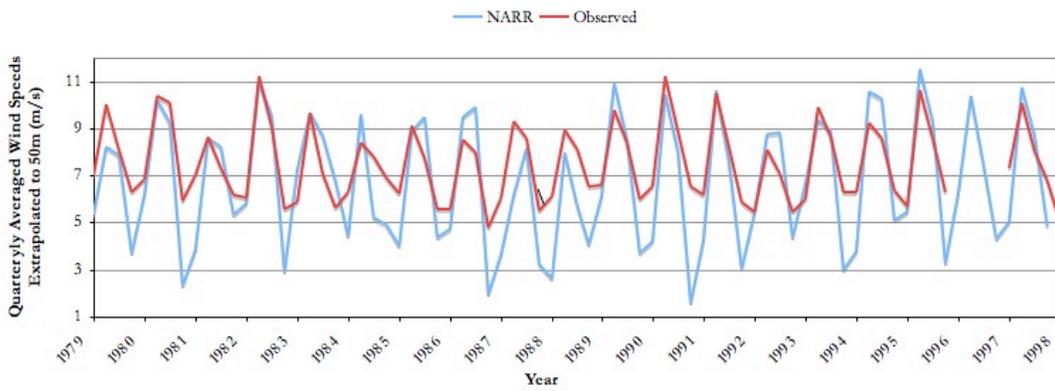
Figure 2.9 is a time series for quarterly averaged wind speeds, in meters per second, extrapolated to a 50 m height for the San Gorgonio wind farm location. The time series runs from the beginning of 1979 to the end of 1998. The observed data is from the Palm Springs International Airport, approximately 9.5 km southeast of the San Gorgonio wind farm. *See Figure 2.1* The observed data measurements are approximately 9.5 km west from the perimeter of the wind farm itself.

The range of wind speeds on this time series is approximately between 3 and 9 m/s with the highest wind speeds from the NARR data set usually occurring in the second quarter of each year. As with the other time series plots, the wind speeds correlate better

during windier months than they do during the times of the year when the wind is not as strong. In the time series plot, the annual variability in the observed wind speeds, overall, correlates well with the NARR data set. The plotted winds trace out each other almost perfectly in the winter months for most of the years. However, discrepancies do exist in the data sets between the years of 1984 and 1985 and between the years of 1987 and 1989. The data during these times does not match up as the observed wind speeds have little annual variability for these years. For the year 1990, the observed winds over shoot the NARR winds during the less windy parts of the year by nearly 6 m/s. The overall correlation between the NARR and observed data sets is .84.

These interannual time series plots show fair a correlation between observed and reanalysis data. Therefore, it can be established that on an interannual basis, the NARR data set is a suitable means for comparing current and historical resources to future projected production in California.

2.9 Spatial Variability of Winds in California

In order to get a spatial and temporal comparison between current and past wind speeds with projected wind speeds, contour filled maps of California were made showing annually and seasonally averaged wind speeds across the state from 1979 to 2008. In doing so, a coarse wind energy assessment map is being made with the NARR data set showing theoretical wind energy power classes.
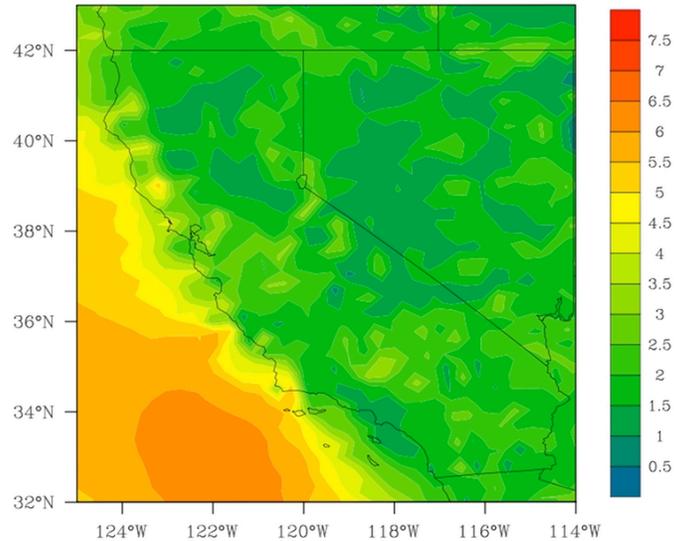
Figure 2.10 Annually averaged NARR 10m surface wind speeds for California from 1979 to 2008 in meters per second

Figure 2.10 is a contour map spatially showing the averaged annual 10 m surface winds for California and surrounding areas for a period of roughly 30 years, from January 1979 to December 2008. The map gives an overall look at the spatial variations in wind speeds across the state, as well as the surrounding regions. It is clear from the map that there exists higher wind speeds over the Pacific Ocean than on land, and that there is a large gradient along the California coast separating the two regions. The range of annually averaged surface wind speeds ranges from 1 to 7.5 m/s. From the annually averaged plot, it seems the NARR does underestimate the winds as most of the areas near the farms lie in spaces where the wind class is 1, or less than 4.4 m/s by Table 1.1. This is much lower than precious studies done by NREL where the surface winds were in optimal power classes 6 and 7. It should be noted that the accuracy of the NARR maps is limited by the 32 km x 32 km resolution of the reanalysis data. Nonetheless, these maps are sufficient tools for comparing current and past wind speeds with projected wind speeds for the middle of the 21st century as changes in the winds can still be seen.

Figure 2.11 is a series of four contour maps spatially showing the averaged seasonal 10 m surface winds of California for the time period of 1979-2008. Each map is for a different season.
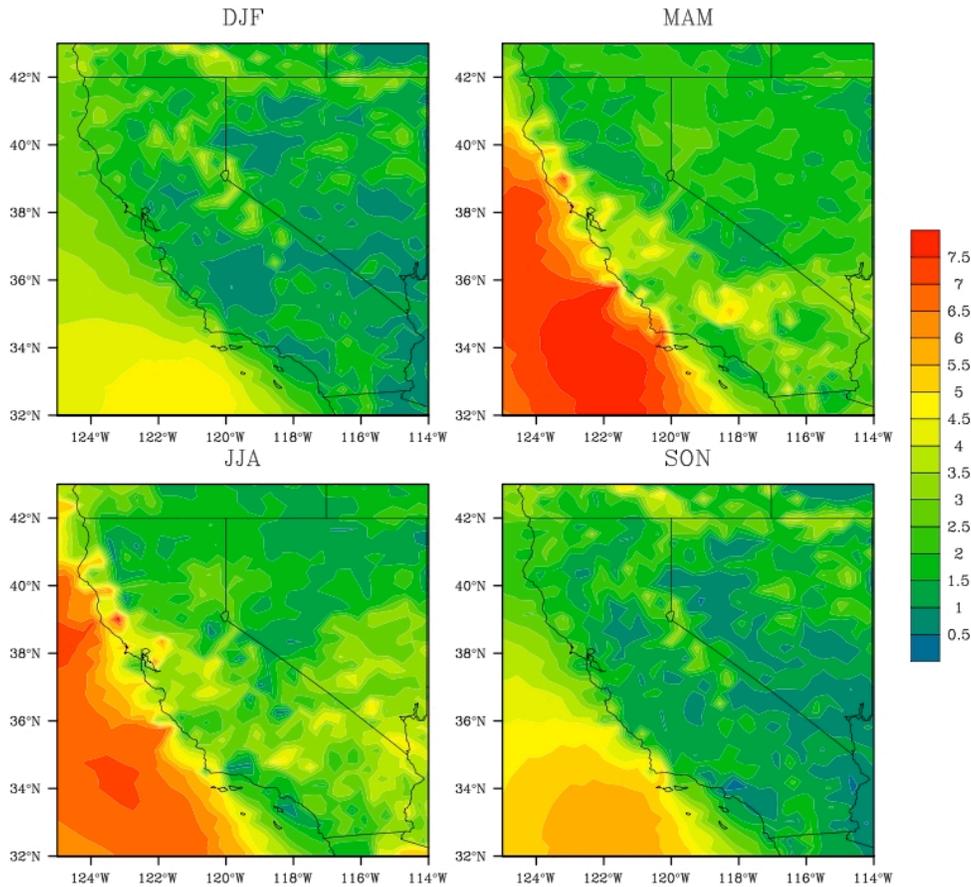
Figure 2.11 Seasonally averaged NARR 10 meter surface wind speeds in meters per second for California from 1979 to 2008

The labels of DJF are for the winter months of December, January, and February, MAM are the spring months of March, April, May, JJA are the summer months of June, July August, and lastly SON are the autumn months of September, October, and November. From the maps, it is clear that the Californian interior experiences the greatest wind speeds in the spring and summer seasons. Correspondingly, in the spring and summer, electricity demand increases for the state of California due to air conditioning and other utility needs. Therefore, the increased wind power production in the spring and summer must play a large

role in mitigating these seasonal electricity demands. This is consistent with electricity production in the past. In 2001, 70% of all of California's wind generated electricity was produced in the second and third quarters *(6)*. It can be seen in Figure 2.11 that calmer wind speeds are present in the winter and autumn seasons, when energy demands are less.

Now that insight into current and past spatial and temporal trends in wind speeds at the wind farm sites has been given, this research will move towards looking at future conditions. The predicted trends in wind speeds generated by the NARCCAP RCMs will be revealed in the proceeding chapter.

3. Projections for Future Winds in California

With an overview of the spatial and temporal characteristics of historical and present winds given in the previous section, a similar analysis of future winds will be discussed here. With an understanding of for seen resources, a means for comparison between future and past conditions will be possible. Objectives in this section include: California climate change outlooks, climate model overviews, and discussions on climate model outputs. The following section of this study will discuss these important transformations in more detail.

3.1 The North American Regional Climate Change Assessment Program

As mentioned previously, climate models will be utilized in this paper to look at transforming conditions in California. Previous works have chosen a variety of different GCM and atmosphere-ocean global climate models (AOGCM) to perform their simulations to get outlooks on wind speeds. Nonetheless, they all chose from many different models, forcings, and boundary conditions. Breslow and Sailor *(8)* chose the Canadian Climate Center (CCC) model and the Hadley Center's model, while Pryor et al. *(11)* chose to use just one RCM, the Rossby Centre coupled regional climate model (RCAO), but with numerous

boundary condition options. These included conditions generated by the

ECHAM4/OPYC3 AOGCM and the HadAM3H atmosphere-only GCM. Pryor et al. *(12)*

utilizes 10 GCMs used in the Intergovernmental Panel on Climate Change (IPCC) 4th

Assessment Report.

However, this paper utilizes some of the most recent and high-resolution

dynamically downscaled climate model runs from the North American Regional Climate

Change Assessment Program (NARCCAP) that are available to the public at this time.

NARCCAP is an internationally driven effort to understand how anthropogenic behavior is

going to impact future regional climates. The program is rooted in a series of four regional

climate models (RCMs) driven by AOGCMs with a corresponding domain over the North

American continent. Nested, or dynamically downscaled, modeling is an appealing way of

simulating winds for wind resource studies due to its ability to create fairly continuous

calculations of wind speeds over a region in focus *(13)*. Segal et al. *(10)* used a similar

AOGCM-RCM model couple to get their winds, the HadCM2 GCM with the RegCM2

RCM nested inside. Nonetheless, before producing future simulations, the NARCCAP

RCMs driven with NCEP Reanalysis II data are tested for their effectiveness by reproducing

historical periods over North America. Thus, instead of using model driven nesting data or

boundary conditions from AOGCMs, reanalysis data was used with these RCMs.

As mentioned, the NARCCAP future climates used in this paper were simulated by

using RCMs driven by AOGCMs. RCMs being driven by AOGCMs are gaining in

popularity in uses where a local simulation is being conducted. The goal in all RCM and

AOGCM setups is lessening the computational strain and increasing the spatial resolution of

the simulation. Ultimately, only two NARCCAP outputs were post processed, quality

controlled, and then made publicly available during the time of this research. These models

are the CRCM+CGCM3 and the RCM3+GFDL. In addition to using the only two models

available, using two models will allow for comparison between outputs, consequently

mitigating the uncertainty in any calculations and projections for future wind availability at

the locations of all three Californian wind farms in this paper.

The NARCCAP data was downloaded in network common data form (netCDF)

format. NetCDF is a data array based interface intended for access with languages such as

C, Fortran, C++, and Java *(38)*. Almost all of the NARCCAP files used include five years of

either the meridional, v, or zonal component, u, of the wind with a time step of every three

hours. The first NARCCAP file from each run only has three years of data. Nonetheless,

for the files with five years of data, every point on the grid has 14600 data values for one

component of the wind; thus, one data value for every three hours over five years. The

NARCCAP data used was downloaded from the Earth System Grid II (ESG) which is a U.S.

Department of Energy (DOE) funded project that is intended to allow smooth and feasible

distribution of climate research data to users *(39)*.

Model:	CGCM3.1 (T47)	GFDL CM2.1
Year and Sponsor:	2005, CCCma	2005, NOAA-GFDL
Ensemble:	CGCM #4	20C3M, run 2
Resolution (lat. x long.):	3.75° long. x lat.	2° long. x 2.5° lat.
Grid Size/NARRCAP domain:	140, 115	104, 134
Vertical Atmospheric Levels:	31 levels	24 levels
Forcing Scenario:	SRES A2	SRES A2

Table 3.1 NARCCAP Atmosphere-Ocean GCM (AOGCM) summary

3.2 NARCCAP SRES A2 Forcing

All of the AOGCM models used with NARCCAP were involved with IPCC

simulations and have extensive histories of accurately reproducing past climates with NCEP

reanalysis data and producing future climates under various forcings with AOGCMs. These

forcings in the AOGCMs are specific scenarios that estimate human activity trends and behaviors that will affect the sources and sinks of green house gases up until the close of the 21st century. The A2 scenario forcing used by NARCCAP is one of the many special reports on emissions scenarios (SRES) devised by the IPCC (IPCC, 2009). Breslow and Sailor *(8)* use a forcing similar to the SRES A2, the IS92a, and Pryor et al. *(11)* utilized the A2 as well as the B2 forcing. Pryor et al. *(12)* used the A2 forcing for all 10 GCM runs.

The A2 scenario is characteristic of a heterogeneous world in which there is less international cooperation, interaction, and economic ties between countries. In this "business as usual" scenario, GHG emissions are high, but not the highest of the multiple SRES outlined by the IPCC. The planetary population of Earth reaches 15 billion by the year 2100 with global GDP simultaneously touching US $250 trillion. The global CO2 concentration in the mid 21st century in the scenario is about 575 ppm and it is roughly 870 ppm at the close of the century *(40)*. For comparison, as of 2009, the global mean CO2 concentration at Mauna Loa, Hawaii is around 390 ppm *(41)*. It has been claimed that a scenario with lower emissions than the A2 could possibly give a vague image of the future for climate impact researchers to study. It should also be mentioned that the A2 scenario does not characterize an *optimistic* or *pessimistic* future, but rather a theoretically possible one with many good and bad characteristics that directly relate to GHG emissions *(42)*. It is impossible to confidently say if this scenario is accurate or not, but it can be said that current trends most closely follow the A2 since its creation by the IPCC *(43)*.

3.3 The CRCM+CGCM3 Coupled Model

The main difference between the two NARCCAP data sets in this paper is the physics and construction of each model from which they are generated. An overview of

both models will be necessary for an understanding of how they operate. This knowledge will consequently substantiate each set of model results produced.

First discussed here is the CRCM+CGCM3 coupled model. Both the Canadian Regional Climate Model (CRCM4.2) and the Coupled Global Climate Model (CGCM3.1) used in this project were developed and created by the Canadian Centre for Climate Modeling and Analysis (CCCma), a division of the Climate Research Branch of Environment Canada.

In order to run the RCM, the CRCM in this case, the boundary conditions must be given for the atmosphere and for the surface. This process is called "nesting". This is where the AOGCM, in this case the CGCM3, comes in. The CGCM3 is responsible for providing the boundary conditions that are used to drive the CRCM. These generated boundary conditions include such variables as, pressure, temperature, water vapor, and horizontal winds. When the model is initiated, it develops its own independent results inside its boundaries. The CGCM3 used in this paper was run with the T47 resolution. Its land surface grid resolution is a 3.75-degree latitude and longitude square and is 31 levels deep in the vertical. The resolution over water is 1.85 square degrees and has 29 vertical levels *(44)*.

The CRCM4.2 used in conjunction with the CGCM3 uses an atmospheric dynamics core that has been building on developments over the past 30 years. Its physical parameterization is based upon the CGCM3 design and the Canadian LAnd Surface Scheme (CLASS 2.7). The CLASS package is a highly detailed modeling component that includes parameters evaluated at minute coordinates. Some examples of inclusion in the CRCM are multiple soil moisture layers that are modeled with thermal characteristics, four varieties of vegetation canopies that can be simulated to catch falling rain and snow, and modeling of

changing lake water temperatures and ice overages. Cleary, the CRCM has the strength to model a future climate accurately *(45)*.

Table 3.2 lists the wind farms and their corresponding grid cells extracted with NCL from the CRCM+CGCM3 data set. Figure 3.1 shows the locations of the wind farms in their corresponding grid cell.

Wind Farm	CRCM+CGCM3 Grid Point Location
Altamont	43, 20
San Gorgonio	30, 27
Tehachapi	34, 24

Table 3.2 Locations of wind farms in CRCM+CGCM3 grid
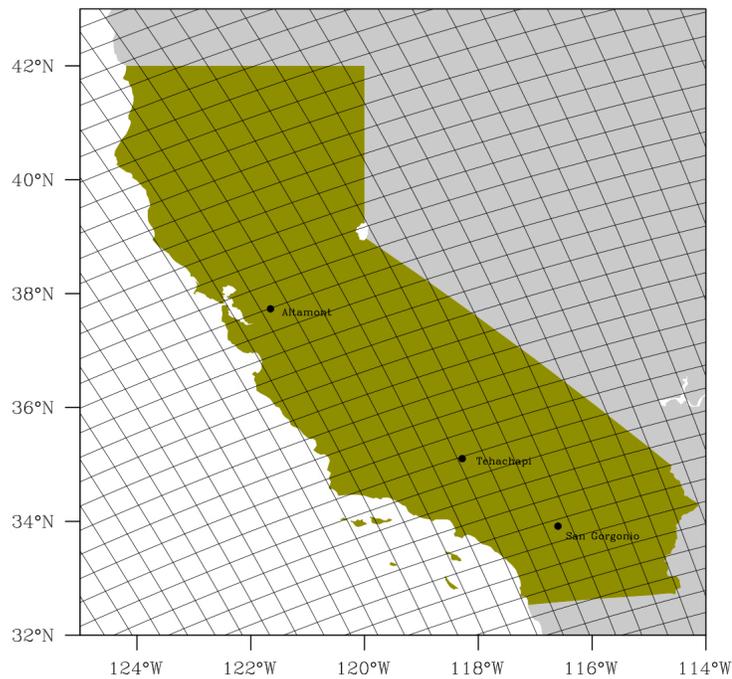
Figure 3.1 The CRCM+CGCM3 model resolution over the state of California showing the CRCM+CGCM3 grid cells and the actual latitude and longitude coordinate locations of the wind farms in their corresponding grid cells

3.4 The RegCM3+GFDL Coupled Model

The other model couple from NARCCAP that is currently available is the RegCM3+GFDL. The RCM used in this coupling is the Abdus Salam International Centre for Theoretical Physics Regional Climate Model 3 (ICTP RegCM3), a third generation RCM ran by UC Santa Cruz. The AOGCM used is the Geophysical Fluid Dynamics Laboratory (GFDL) CM2.1 driver *(46)*.

GFDL is a division of the National Oceanic and Atmospheric Administration (NOAA) and is a leader is the study of modeling complex interactions between the atmosphere and the ocean. The GFDL CM2.1 has a land and atmosphere top resolution of 2 degrees by 2.5 degrees and an ocean resolution of .3 degrees by 1 degree *(46)*.

The RegCM3 dynamic core is the hydrostatic mesoscale model fifth-generation (MM5) developed by Pennsylvania State University and NCAR. The RegCM3's implementations have recently been extended to societal and economic impacts of regionally based climate changes and variations *(47)*. Its use for evaluating the future of wind energy in California is just another example of its many possible uses.

Table 3.3 lists the wind farms and their corresponding grid cells extracted with NCL from the RegCM3+GFDL data set. Figure 3.2 shows the locations of the wind farms in their corresponding grid cell.

Wind Farm	RegCM3+GFDL Grid Point Location
Altamont	36, 23
San Gorgonio	29, 27
Tehachapi	25, 29

Table 3.3 Locations of wind farms in RegCM3+GFDL grid
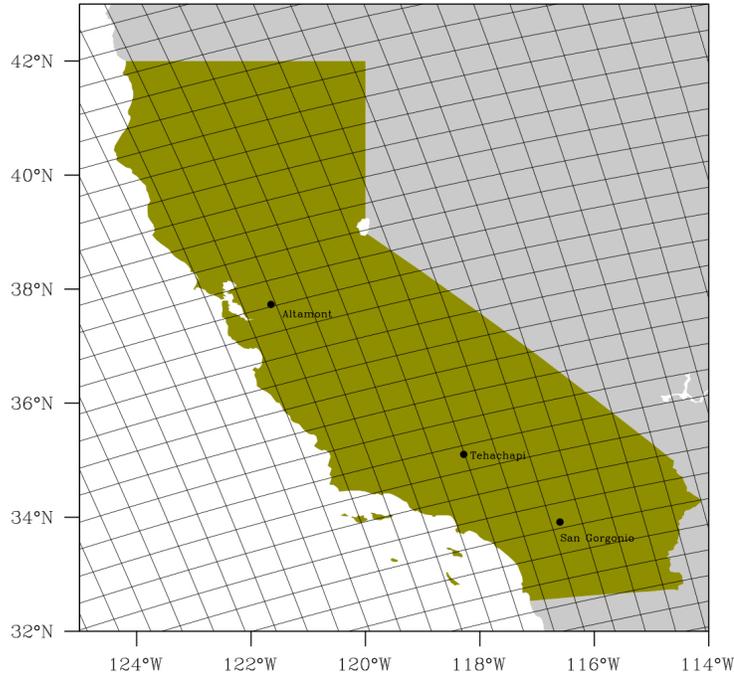
Figure 3.2 The RegCM3+GFDL model resolution over the state of California showing the RegCM3+GFDL grid cells and the actual latitude and longitude coordinate locations of the wind farms in their corresponding grid cells.

3.5 NARCCAP Model Resolutions

On the CCCma model site, it is advised and reminded that climate models only attempt to represent climate systems on large spatial scales to only a first degree. The disclaimer makes note of using caution when comparing climate model outputs with observations on scales smaller than 150-200 km. It further announces that one should be mindful when utilizing model output to study the impacts of climate change *(44)*. This problem is clarified in Table 3.4 where it can be seen that the scales of the wind farm's approximated areas are an order of magnitude smaller than that of the model resolution area.

Model	Resolution	Area
CRCM4.2.3	45km x 45km	2025 km^2
RegCM3	50km x 50km	2500 km^2
NARR	32km x 32km	1024 km^2

Table 3.4 Model resolutions and their corresponding areas

The wind farm areas in Table 3.5 have been estimated with the use of aerial maps (Figures 2.1 - 2.3).

Wind Farm	Approximated Area
Altamont Pass	312.2 km^2
San Gorgonio	202.63 km^2
Tehachapi	291.8 km^2

Table 3.5 The Wind farms and their corresponding areas

In addition, all of California's wind farms are in areas where the terrain makes it difficult to simulate surface airflows. It is especially difficult to model the flows at the locations of the wind farms when the terrain complexities are on scales of the model's grid or smaller. For example, San Gorgonio Pass, where the San Gorgonio wind farm is located, has a width of only a couple kilometers. For a model to accurately determine the actual circulations of the pass, the resolution needs to be around 5 km. In addition, at some of California's wind farms, some the turbine units are located on the tops of ridgelines. It is known that vertical accelerations are present at locations of steep terrain. This is why the turbines were sited where they are, for the purpose of utilizing the amplification of the flows. This phenomenon ultimately defies traditional hydrostatic balance, where the force of gravity is balanced with the pressure gradient in the vertical. Therefore, using non-hydrostatic models to recreate the actual flows at such wind farms might be a way to obtain more realistic wind speeds *(17)*.

3.6 RCM and AOGCM Downscaling Methods

Nonetheless, it is expected that AOGCM models will give inaccuracies, as their respective resolutions, topography, and physics parameterizations are fairly insufficient for simulating 10 m surface winds. RCM and AOGCM coupled models are generally able to predict large-scale climatic variables much more accurately. Techniques such as wind speed

statistical, or empirical, downscaling done by Pryor et al. *(11, 12)* have been able to greatly increase the spatial resolution of winds at the surface from RCMs for a specified domain. Pryor et al. *(12)* found correlation between observed mean and 90th percentile wind speeds for 45 sites and downscaled winds from 10 control GCM runs to exceed 0.99.

Statistical downscaling was also utilized by Sailor et al. *(13)* with coarse resolution GCM model output from IPCC runs in a wind energy climate impact assessment study done for the Pacific Northwest. Sailor et al. found that without downscaling, the GCMs gave grossly inconsistent and unrepresentative values for wind speeds in the areas of study. Consequently, the application of statistical downscaling to the model output greatly improved the accuracy of these winds from the GCMs.

However, in different research, downscaling done by Miller et al. *(48)* had better results reproducing historical California surface winds with dynamical downscaling than they did with statistical downscaling. Nonetheless, Miller et al *(48)* only briefly mention their past climate wind reproduction results with the downscaling from the RegCM3 and WRF models. Instead, they primarily focus on the dominant seasonal surface wind circulation. It is mentioned that a more detailed analysis of the reproduced winds is forth coming.

The use of RCM and AOGCM coupled models ran by NARCCAP used in this paper are a rudimentary form of dynamical downscaling. More complex methods, such as statistical downscaling, are beyond the scope of this paper and will not be utilized. They should be considered for future work in this particular research, as it has been shown by Pryor et al. *(11)* that it is an excellent method to increase the spatial resolution of modeling wind speeds.

3.7 Interannual Variability of the NARCCAP Models

In an effort to get a better understanding of the year-to-year variability in the winds at the Californian wind farms and between the wind farms in the middle of the 21st century, time series plots were created. Pryor et al. *(11)* stressed the importance of temporal variations in modeled future wind speeds, on time scales of decades, in their concluding remarks. These plots presented here are similar to the NARR time series figures in the previous section.

Figure 3.3 is a set of time-series plots for Altamont, San Gorgonio, and Tehachapi Pass winds, quarterly averaged, from the CRCM+CGCM3 in meters per second and extrapolated to 50 meters. Overall, the wind speeds don't show an obvious trend, as they stay relatively constant over the mid 21st century. Yet, year-to-year wind speed variability seems to be much less in Figure 3.3 in comparison to the NARR plots of interannual wind speed variability, Figures 2.7-2.9.
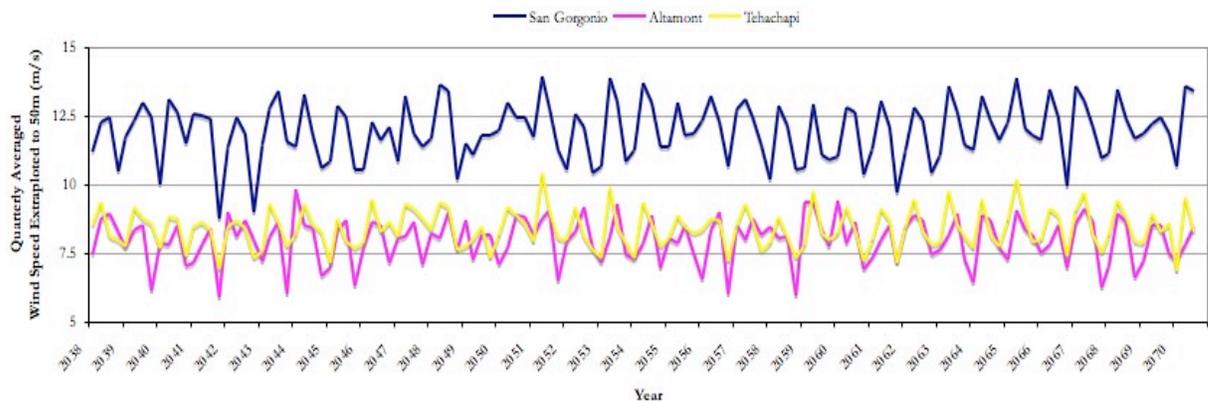

Figure 3.3 Time series plot of CRCM interannual variability of 50-meter wind speeds in meters per second for San Gorgonio, Altamont, and Tehachapi Pass.

In most years in Figure 3.3, winds maximally vary by only 2 to 3 m/s. Also in Figure 3.3, the two consecutive quarters of high wind speeds often seen in the NARR time series plots,

denoted by the "flat tops" on the each annual wind speed peak, are mostly absent. However, two consecutive quarters of high wind speeds do appear in such years as 2048 and 2060.

In addition, in Figure 3.3 it can be seen that the San Gorgonio Pass winds from the CRCM shows a higher wind speed bias compared to Altamont and Tehachapi Pass. Despite this, Figure 3.4 shows good interannual correlation in wind speeds between San Gorgonio and Tehachapi Pass. This statistical artifact may be related to the fact that these wind farms are in relatively close proximity to one another and thus correspondingly experience similar meteorological forcings in the RCM. The interannual correlation between Altamont Pass and the Southern California wind farms is fair, showing a positive correlation for most of the mid-21st century.
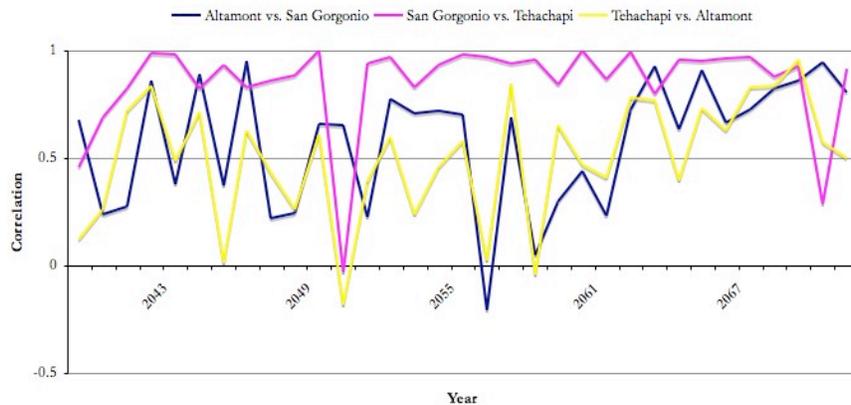
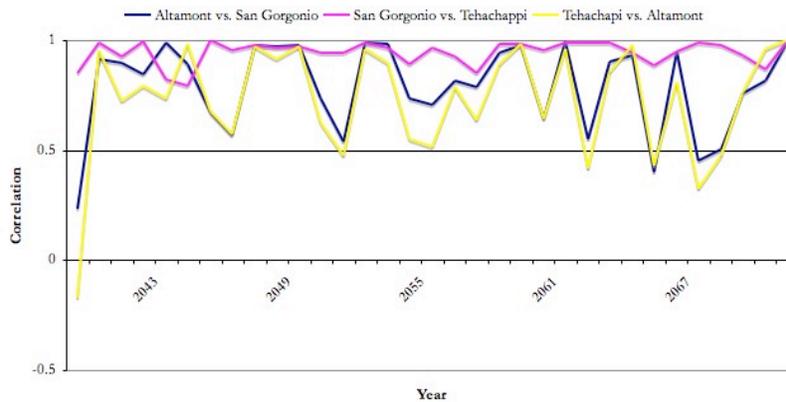*Figure 3.4 Interannual variability of correlation between CRCM wind speeds at the wind farms*

Like Figure 3.3, Figure 3.5 is a time series with RegCM3+GFDL data. Wind speeds from the RegCM3+GFDL at the wind farm locations also don't reveal any signatures that can be considered an obvious mid-21st century trend. All three of the Californian wind farms are shown with very similar wind speed magnitudes and interannual variability. Like

Figure 3.3, the sites exhibit a few consecutive quarters of high winds, indicated by the "flat

tops", but not as many as seen in the NARR interannual plots.
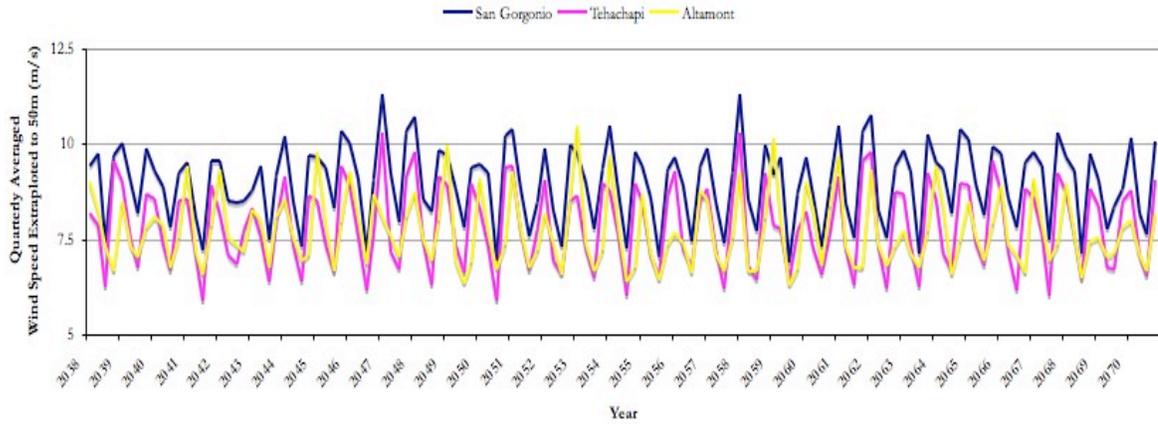
Figure 3.5 Time series plot of RegCM3 interannual variability of 50-meter wind speeds in meters per second for San Gorgonio, Tehachapi, and Altamont Pass

Figure 3.6 also shows excellent interannual correlation between the sites as well, with

correlation primarily staying above .5. San Gorgonio and Tehachapi Pass have almost a

consistent correlation of 1 through out the mid 21st century. It's clear that the

RegCM3+GFDL wind speeds show a much more uniform relation between the respective

wind farms.

*Figure 3.6 Interannual variability of correlation between RegCM3 wind speeds at the wind farms*

3.8 Future Spatial Variability of Winds in California

Figure 3.7 is a contour plot of CGCM3+CRCM averaged 10-meter wind speeds for California for roughly the mid-21st century, 2038-2070. It can be seen that the interior wind speeds are greatest in the southern half of the state, below about 36 degrees North latitude. Shown in this particular region are winds ranging from 0.5 m/s to 4 m/s. In this same region in Figure 2.10, the NARR averaged 10-meter winds from 1979-2008, the winds appear less variable, ranging from 1.5 to 4.5 m/s. Overall, the wind speeds appear more variable across the state than in the NARR data set with a more uniform stronger gradient of surface wind speeds along the coast. However, due to its coarser resolution, the CRCM+CGCM3 does not reproduce the finer spatial variations in surface wind speeds that can be seen in the high resolution NARR data set plot. Importantly, it should be noted that all of these plots given in this paper might neglect finer scale variations that exist in the actual wind speed data sets. This issue maybe due to NCL's grid cell interpolation methods that are used to plot contour maps
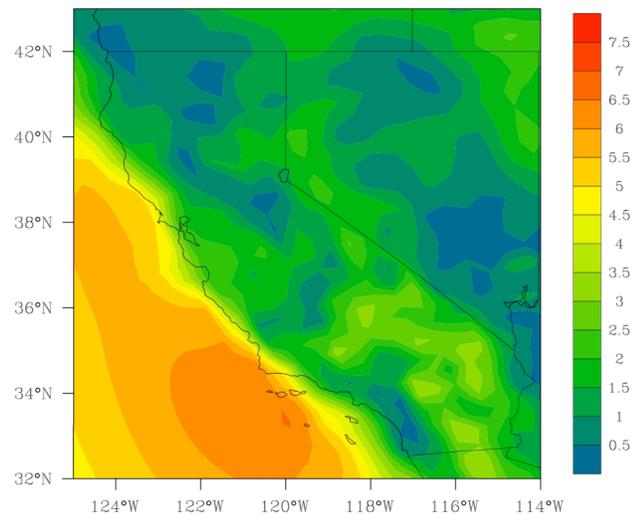
Figure 3.7 is an annually averaged 10-meter surface wind speed contour plot from the CGCM3+CRCM for California for the years 2038-2070 in meters per second.

Figure 3.8 is a contour plot of RegCM3+GFDL averaged 10 m surface wind speeds for California for roughly the mid 21st century, 2038-2070. From Figure 3.8 it can be seen that, spatially, the RegCM3+GFDL predicts significantly slower averaged wind speed magnitudes over California and the Pacific Ocean. Overall, winds from the RegCM3+GFDL are much slower than that shown in the NARR averages plot, Figure 2.10. However, like the CRCM+CGCM3, the highest averaged surface winds are predicted to again occur in the Southern half of California. The variability from the RegCM3+GFDL is also the weakest out of all the data sets with winds over the state ranging from 0.5 to 3.5 m/s.
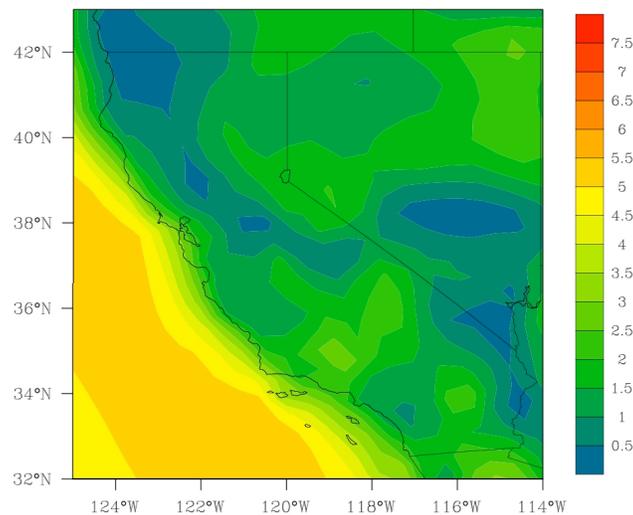
Figure 3.8 is a contour plot of annually averaged RegCM3+GFDL 10-meter surface wind speed contour plot for California for the years 2038-2070 in meters per second.

However, due to its coarser resolution, the RegCM3+GFDL does not reproduce the finer spatial variations in surface wind speeds that can be seen in the higher resolution NARR data set plot.

The predicted seasonally averaged 10-meter surface wind speeds from the CRCM+CGCM3 are given in Figure 3.9. Wind speeds range 0.5 m/s to over 8.0 m/s.

Winds over the Pacific Ocean are consistently higher than they are over the state of California. It can been seen that, overall, wind speeds are predicted to somewhat continue to follow the 1979-2008 average annual trend with maximum winds occurring in the summer and spring months and with lower wind speeds occurring in the autumn and winter.
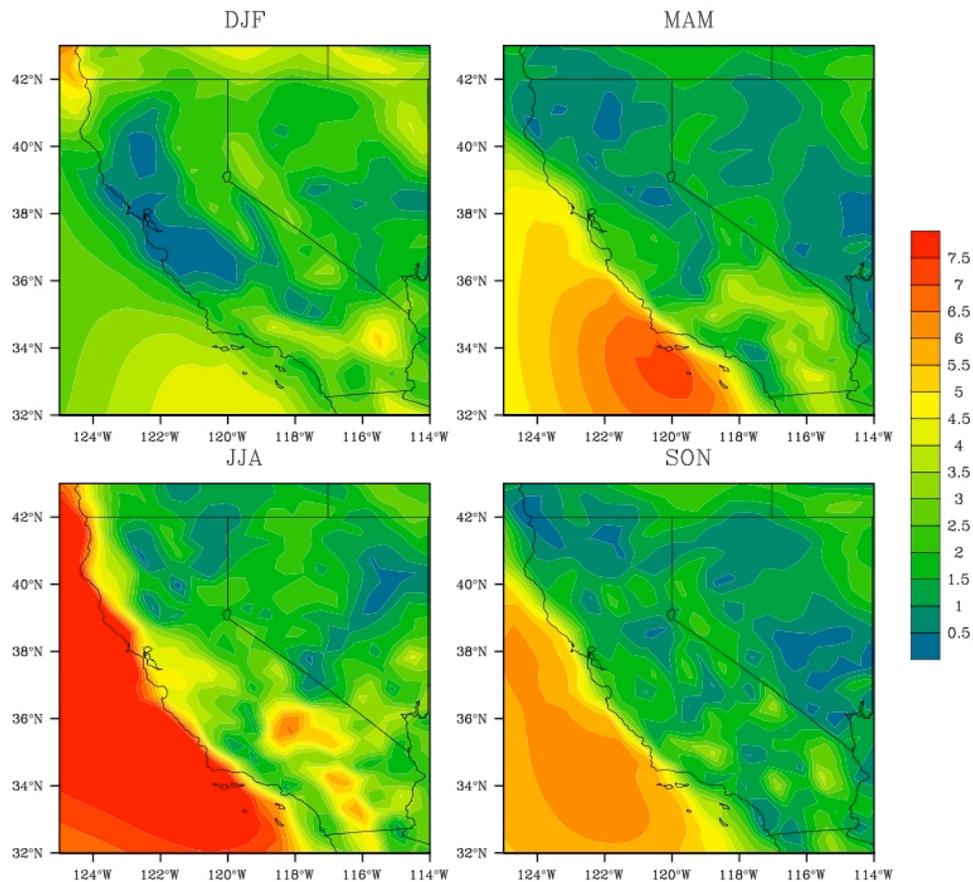
Figure 3.9 Seasonally averaged CRCM+CGCM3 10 meter surface wind speeds in meters per second for California from 2038-2070.

However, the CRCM+CGCM3 does predict an annual wind speed maximum in JJA, rather than the 1979-2008 NARR maximum in MAM seen in Figure 2.11. The CRCM+CGCM3 also predicts higher wind speeds to occur in the interior of California in JJA. The NARR data set has its seasonal maximum in interior winds in MAM. During the winter months, the gradient of mean wind speeds between the Pacific and California relaxes as it does in the NARR data set, indicative of the thermal gradient relaxing between the land and ocean. *As a*

note, data for December 2070 from CRCM+CGCM3 was not available during the time of this study and is not included in any plot or calculation.

The predicted seasonally averaged 10 m surface wind speeds from the RegCM3+GFDL are given in Figure 3.10. Wind speeds range from 0.5 m/s to over 8.0 m/s. As in the CRCM+CGCM3 and NARR contour plots, the winds over the Pacific Ocean are consistently higher than they are over the state of California.

Figure 3.10 Seasonally averaged RegCM3+GFDL 10 meter surface wind speeds in meters per second for California from 2038-2070.

Again, wind speeds are predicted to somewhat continue to follow the NARR 1979-2008 average annual wind speed trend with maximum winds occurring in the summer and spring months and with lower wind speeds occurring in the autumn and winter. Like the
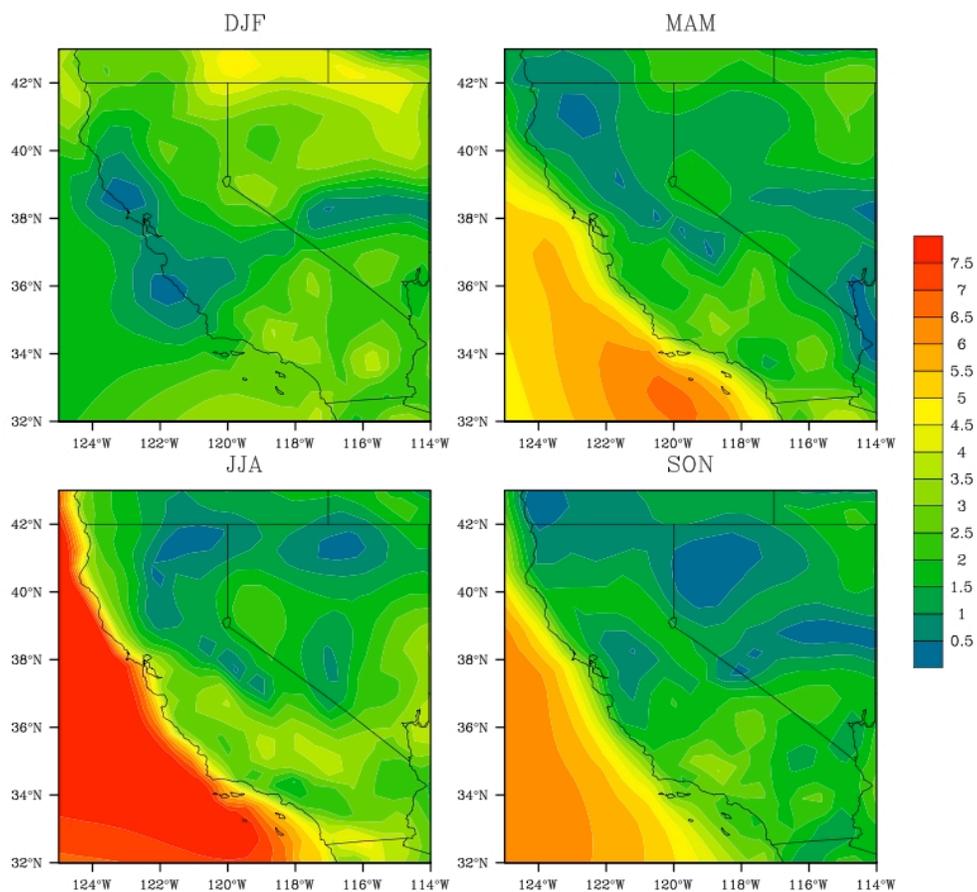
CRCM+CGCM3, the RegCM3+GFDL also predicts an annual wind speed maximum in JJA, rather than the 1979-2008 maximum in MAM in the NARR data set seen in Figure 2.11. The RegCM3+GFDL predicts higher wind speeds to occur in the southern half of the interior of California in JJA and, interestingly, DJF. These DJF interior predicted winds are anomalously higher than those in the other data sets. But despite the increase in interior wind speeds in DJF, the gradient of mean wind speeds between the Pacific and California relaxes much more considerably than it does in the NARR and CRCM+CGCM3 data sets. As mentioned previously, finer detailed spatial variability artifacts in Figures 3.9 and 3.10 may come at a cost of NCL's grid cell interpolations.

4. Changes Between Past, Current, and Future Winds

Thus far, only wind speed data has been presented from the past, present and from the projected future. They all have been examined in aspects of spatial and temporal variability. By analyzing these multiple datasets simultaneously in this section, it is hoped that clear conclusions regarding expected changes between current and future resources can be achieved. It is these changes that California's wind energy industry will be requiring adapt to—the greater the change, the greater the adaptation needed. Specifically, this section will be focused on evaluating both the overall frequency and the annual variability of wind speeds at the wind farm sites.

4.1 Wind Speed Frequencies

Considering the high variability of 3 and 6-hour wind speeds over a period of several years, wind speed distributions can be utilized to gain an insight into the frequencies or prevalence of the amount of resources at each site. Taking an average of wind speeds alone cannot reveal a conclusion about the availability of ideal wind resources necessary to generate power. Breslow and Sailor *(8)* acknowledge that more "confidence" can be relied

upon in "predicted changes in wind fields" rather than an "absolute prediction" in the "winds themselves". Looking at the entire wind field values over a long time span in the proceeding frequency plots will give insight into the important changes that Breslow and Sailor *(8)* refer to.

Figure 4.1 is a series of plots of 50m extrapolated wind speed frequencies in m/s from the data sets of the NARR, in blue, RegCM3, in green, and the CRCM, in red.

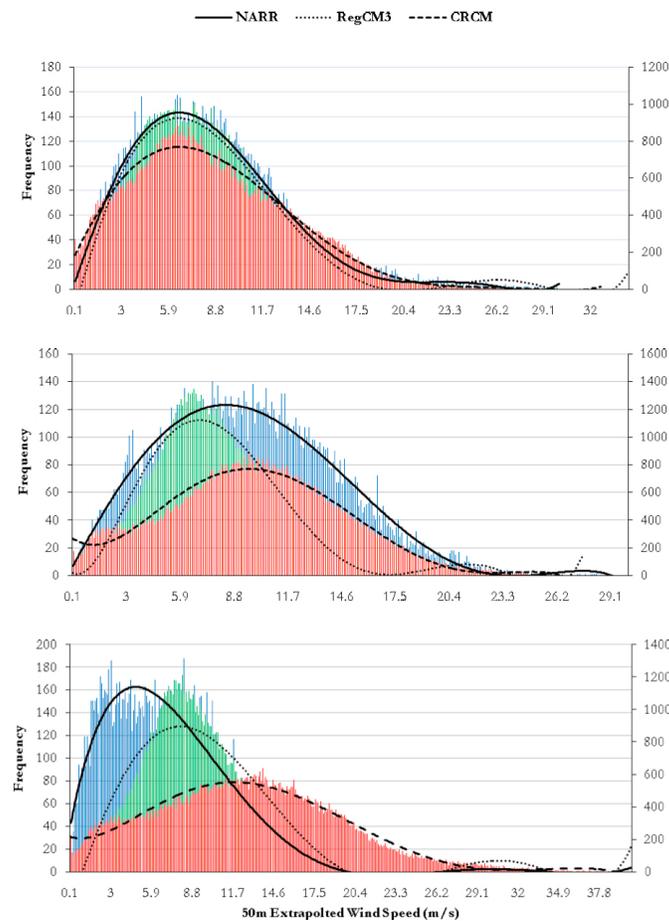***Figure 4.1 are plots of frequency of 10m wind speeds (m/s) from the NARR (blue) RegCM3 (green) and CRCM (red) data sets. Locations are, from top to bottom, Altamont Pass, Tehachapi Pass, and San Gorgonio Pass. Curves plotted are fitted to the data sets. Solid curve is fitted to the NARR data set, the dotted curve is fitted to the RegCM3 data set, and the dashed curve is fitted to the CRCM data set.***

The NARR frequencies correspond to 6-hour winds from 1979 to 1989 and they are plotted on the left hand y-axis. The daily hours used were from 00, 06, 12, and 18 UTC. Since individual data files for every 3 hours were available, only a selected amount of data was downloaded due to computational constraints related to the data extraction with NCL and due to downloading constraints from the Earth System Research Laboratory (ESRL). Such constraints were not an issue with the monthly averaged NARR data used in this paper, as there were much fewer files to download. Thus, all years from 1979-2008 were applied in the cases where monthly data made used.

However, the NARCCAP data used in Figure 4.1 are wind speeds from every 3 hours from the mid 21st century period of 2038-2070. The CRCM and RegCM3 data sets from NARCCAP extracted wind speeds much easier computationally than the NARR, and the fact that the data is contained in only a few files made it easier to plot. The frequencies of the future winds are plotted on the right hand y-axis. Wind speed frequency curves were also plotted by fitting a six-order polynomial to the data sets. The curves give a clearer comparison of the distributions. The solid curves correspond to the NARR data set, the dotted curves to the RegCM3, and the dashed curves to the CRCM. It can be seen from the first plot in Figure 4.1 that there is little change expected in the distribution of wind speeds at Altamont Pass. However, the CRCM is predicting a slight decreased frequency of lower winds speeds around 7 m/s and a slight increased frequency of higher wind speeds around 15 m/s. At Tehachapi Pass, the CRCM is predicting an increase in the frequency of wind speeds in excess of 10 m/s. The RegCM3 gives the opposite, a decrease in the availability of wind speeds higher than 6 m/s. The CRCM at San Gorgonio Pass is predicting a very large increase in overall wind speed and an increase in the frequency of higher wind speeds. In

addition, the RegCM3 assesses an increase in wind speeds and the frequency of these higher

winds as well, but does not have as big of an amplification as the CRCM.

4.2 NARCCAP, NARR, and Observed Annual Temporal Variability

Figure 4.2 is a plot of averaged wind speeds in meters per second from observed,

NARR, CRCM, and RegCM3 data sets for the Tehachapi Pass wind farm area.
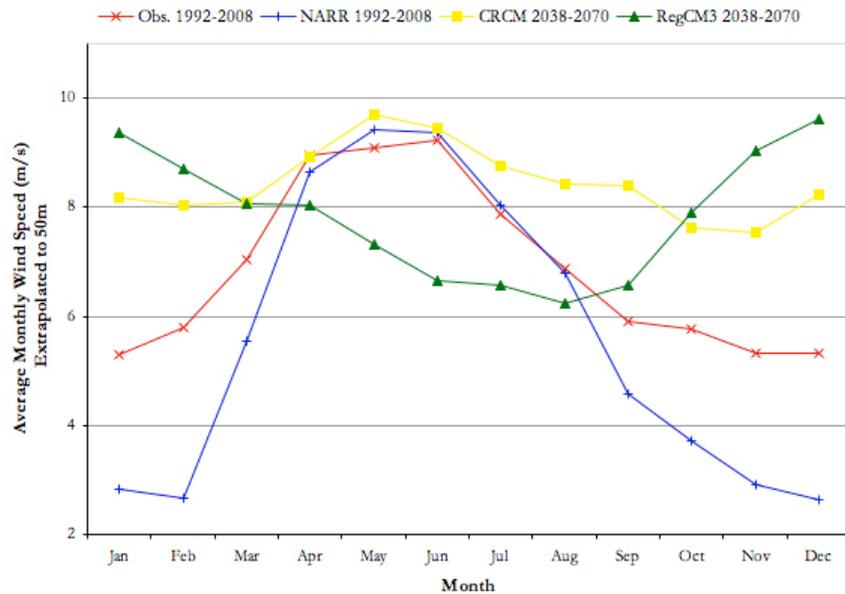
Figure 4.2 Plotted wind data sets for observed, NARR, CRCM, and RegCM3 annual variability of wind speeds in meters per second for Tehachapi Pass

The observed and NARR data sets are plotted as a baseline for comparison to the two

RCM-AOGCM coupled runs. The baseline data sets have much more annual variability

compared to the CRCM and RegCM3 runs. However, the trends in annual wind speeds

seem to be consistent between the observed, NARR, and CRCM. For example, these data

sets have the highest winds occurring in the second quarter of the year during April, May,

and June with values around 9 m/s, in wind power class 7. This can be verified spatially by

viewing the CRCM seasonally averaged surface wind speeds in Figure 3.9 and the NARR in

Figure 2.11.

However, the RegCM3 is the exception to this trend as its annual signature is nearly opposite to the other plotted data sets. It experiences the lowest wind speeds in the third quarter of each year and the highest wind speeds during the months of November, December, and January. The difference in wind speeds between the RegCM3 and the NARR data sets is nearly 6 m/s during January and December, and about 2 m/s during May through August. The maximum speed of the RegCM3 winds is around 10 m/s and the lowest value is around 6 m/s. It will be shown in the proceeding plots that the RegCM3 continues to give this opposite annual trend in the location of the other wind farms.

The CRCM run shows the least annual variability in wind speed, but gives a maximum for the months of April, May, and June, consistent with the baseline observations. The minimum CRCM wind speeds occur in the month of November and are around 7-8 m/s, a significantly high annual minimum. Thus, the monthly averaged CRCM resources never drop below wind power class 4 and 5.

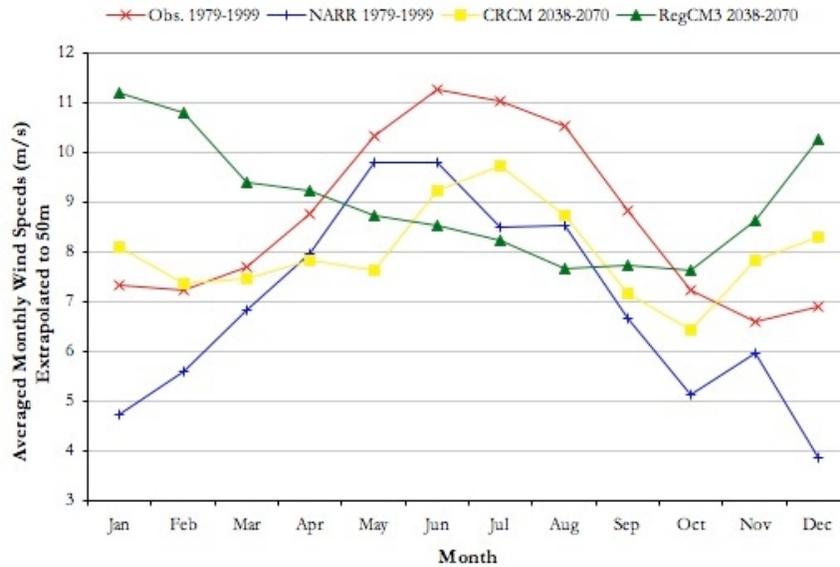Figure 4.3 is a plot of averaged wind speeds in meters per second from observed, NARR, CRCM, and RegCM3 data sets for the Altamont Pass wind farm area. Again, the observed and NARR data sets are plotted as a baseline for comparison to the two future climate runs.

Figure 4.3 Plotted wind data sets for observed, NARR, CRCM, and RegCM3 annual variability of wind speeds in meters per second for Altamont Pass

As shown, the baseline data sets have much more annual variability compared to the CRCM and RegCM3 runs with the NARR winds, averaged from 1979-1999, varying annually from about 4 m/s to nearly 10 m/s and the observed winds, averaged also from 1979-1999, varying annually from around 7 m/s to around 11 m/s. The monthly averaged observed winds never fall below wind power resource class 4 at Altamont Pass. Nonetheless, the peak wind speeds for the baseline data sets are in the second quarter of the year for the NARR and in the summer months of June, July and August for the observed winds. The projected wind speeds from the CRCM are expected to be highest in the summer months, and lowest in the autumn months of September, October, and November; this is supported by the contour plots of seasonally averaged wind speeds in Figure 3.9. The CRCM and RegCM3 both predict an increase in wind speeds during the winter months in relation to the baseline winds. More specifically, the RegCM3 indicates a rough increase in wind speeds of around 6 m/s in January alone from the baseline, and the CRCM a rough increase of 4 m/s in January from the baseline. The RegCM3 also again shows an unusual averaged annual wind speed

49

signature with speeds peaking in the winter months and decreasing to a minimum in August, September, and October, roughly at the same time where the CRCM indicates a predicted decrease in wind speeds.

Figure 4.4 is a plot of averaged wind speeds in meters per second from observed, NARR, CRCM, and RegCM3 data sets for the San Gorgonio Pass wind farm area. Again, the observed and NARR data sets are plotted as a baseline for comparison to the two RCM-AOGCM coupled runs. As shown, the NARR data set has the most annual variability compared to the observed, CRCM, and RegCM3 runs. The NARR winds, averaged from 1979-1998, vary annually from about 3 m/s in December to between 10 and 11 m/s in May and June.

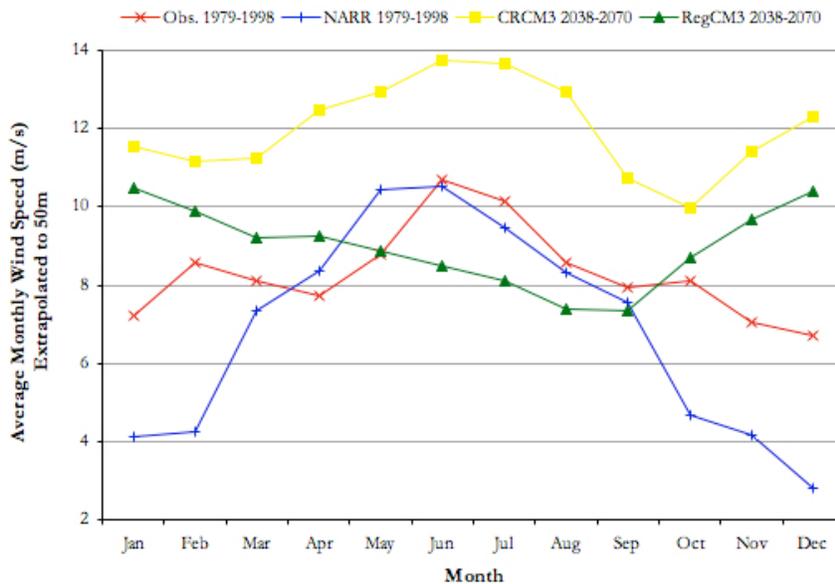*Figure 4.4 Plotted wind data sets for observed, NARR, CRCM, and RegCM3 annual variability of wind speeds in meters per second for San Gorgonio Pass*

The observed winds, averaged also from 1979-1998, annually vary from around 7 m/s in January and December to around 11 m/s in June, again never falling below wind power class 4 during the year as is the case with the observed winds at Altamont Pass seen in Figure 4.3.

Nonetheless, the peak wind speeds for the baseline data sets are in the second quarter of the year for the NARR and for the observed winds. Noted here are the highly biased wind speeds from the CRCM projecting high wind speeds that are greater than the other data sets at any other time during the year. Yet, the CRCM signature is comparable to the other data sets as the highest wind speeds are in the spring and summer months and lower winds are in the autumn and winter. This can be verified by spatially viewing the CRCM seasonally averaged surface wind speeds in Figure 3.9. The CRCM and RegCM3 both predict an increase in wind speeds during the winter months in relation to the baseline winds. More specifically, the RegCM3 indicates an increase in wind speeds roughly around 6 m/s in January compared to the NARR baseline and also a change of roughly 3 m/s from the observed baseline. The RegCM3 again shows the unusual averaged annual wind speed signature with resources peaking in the winter months and decreasing to a minimum in August and September, roughly the same time where the CRCM data set indicates a predicted annual minimum in wind speed.

4.3 Discussion of Findings

This assessment of mid-21st century wind speeds at California's largest wind farms has shown that an anthropogenically induced global climate change will undoubtedly change current spatial and temporal patterns of winds. Other authors report similar results. With empirical downscaling amongst an ensemble of models, Pryor et al. *(12)* were able to report that there is a ±15% change between mid-21st century and late 20th century winds over Northern Europe. In previous work, they also support the importance of considering the variations in large-scale simulated climate by AOGCMs *(11)*. Sailor et al. *(13)* conclude a possible 40% reduction in summertime wind energy production in the Pacific Northwest resulting from SRES impact scenarios. Segal et al. *(10)* conclude annual wind climatology

changes over the US to amount to ±10% in the mid-21st century with a global atmospheric CO_2 increase. They found seasonal resources in most areas to decrease between 0-30%, but isolated regions have increases between 0-30% as well. However, Segal et al. *(10)* do caution that their research should be considered "exploratory". Breslow and Sailor *(8)* concluded similar exploratory findings as they acknowledge a large degree of uncertainty remained between their two model's results. Their study did show a 1-45% reduction in winds over the 21st century, but the GCM data was not downscaled and thus their results cannot be considered substantially accurate for the future. In this study, more sophisticated downscaling techniques and models would have been useful for increasing the spatial resolution of the predicted winds.

This report reveals that the temporal variability of future winds is expected to be altered from their current state. More specifically, the NARCCAP interannual time series plots show less frequent occurrences of two consecutive quarters of high wind speeds compared to the NARR and observed data sets. Again, the "flat tops" of the annual wind speeds in the time series plots indicate these particular events. In addition, both NARCCAP models do show an increase in the average annual wind speeds in the winter months over the baseline resources available at the wind farms. Sailor et al. *(13)* also report similar findings as they reveal an 80% increase in wintertime winds over their baseline amounts from the GFDL GCM for a specific site in the Pacific Northwest. All other sites in their study show a decrease year round, but a smaller decrease is present in the wintertime winds.

Although temporal variability changes are expected, the changes in the annual variability of wind energy production from the two NARCCAP coupled models used in this study are inconclusive. The CRCM, overall, predicts a continuation of the observed trend

with a peak in wind speeds in the summer, while the RegCM3, overall, predicts a peak in wind speeds in the winter months with lower wind speeds in the summer. . In this research, more NARCCAP models would have been useful, if available. This would have mitigated the uncertainty present in the above-mentioned results where two distinctly opposite annual variability signatures exist in the two data sets used.

5. Conclusion

This study has shown that these changes in resources will not be uniform and consequently will vary at the wind farm locations across the state of California. Investors in wind energy should consider the findings presented, as the power production resulting from wind is a function of the cube of the available winds. Thus, even very small changes in wind speed can be amplified to costly gains or losses in utility company profits and production yields.

The increases in both wind speed and high wind speed frequency assessed at San Gorgonio Pass are of particular interest as both the CRCM and RegCM3 models are in agreement that there will significantly more wind resources available at this site in the mid - 21st century compared to both observed measurements and reanalysis data from the past 30 years. The overall changes of wind resources at Altamont and Tehachapi Pass are less conclusive given by the results in Figure 4.1. Here the two NARCCAP models show a less obvious transformation from the baseline resources, as they seem to respectively show both a decrease and increase in the frequency of the availability of higher power class resources. Therefore, at these locations there seems to be no evidence to either undoubtedly support or not support future production at Altamont and Tehachapi Pass based on results given in this study.

Nonetheless, it seems that wind generated electricity in California will remain a reliable means of renewable energy well into this century and will be quite resilient to possible decreases in year-to-year resources from a changing climate. As such, the 21st century's climate should not endanger wind's contribution towards Executive Order S-14-08 and other future wind energy investments in the state of California.

References

(1) Office of the Governor. Press Release: "Gov. Schwarzenegger Issues Executive Order Directing State Agencies to Plan for Sea Level Rise and Climate Impacts."; 2008; available at http://gov.ca.gov/press-release/11035/.

(2) American Wind Energy Association. "2008: Another Record Year for Wind Energy Installations"; 2008; available at http://awea.org/pubs/factsheets/Market_Update_Factsheet.pdf.

(3) California Energy Commission. Overview of Wind Energy in California; 2009; available at http:// energy.ca.gov/wind/overview.html.

(4) _____. California Climate Adaptation Strategy Discussion Draft; 2009; available at http:// climatechange.ca.gov/adaptation/count/click.php.

(5) _____. Wind Energy in California; 2009; available at http:// energy.ca.gov/wind/.

(6) Yen-Nakafuji, D. (2005) Research and Development Office Technology Systems Division. California Energy Commission. California Wind Resources; 2005; available at http:// energy.ca.gov/2005publications/CEC-500-2005-071/CEC-500-2005-071-D.PDF.

(7) Houghton J.T.; Meria Fiho L.G.; Callander B.A.; Harris N.; Kattenberg A.; Maskell K.; editors. *Climate change 1995 — the science of climate change*, Cambridge University Press: Cambridge, UK, 1996.

(8) Breslow, P.B.; Sailor, D. J. Vulnerability of wind power resources to climate change in the continental United States, *Renewable Energy* **2002**, 27 (4), 585-598.

(9) NREL. Renewable Resource Data Center. Wind Energy Resource Atlas of the United States: Table 1-1 Classes of wind power density at 10 m and 50 m; 1983; available at http://rredc.nrel.gov/wind/pubs/atlas/tables/A-8T.html.

(10) Segal, M. et al., On the potential change in wind power over the US due to increases of atmospheric green house gases, *Renewable Energy* **2001**, 24, 235–243.

(11) _____; Barthelmie, R. J.; Kjellström, E. Analyses of the potential climate change impact on wind energy resources in northern Europe using output from a Regional Climate Model, *Clim. Dyn.* **2005** 25 (7-8), 815-835.

(12) Pryor S.C.; Schoof J.T.; Barthelmie, R.J. Winds of change? Projections of near-surface winds under climate change scenarios. *Geophysical Research Letters* **2006** 33, L11702.

(13) Sailor, D.J.; Smith M.; Hart M.; Climate change implications for wind power resources in the Northwest United States. *Renewable Energy* **2008** 33, 2393-2406.

(14) NOAA and Ruffner, J. A. *Climates of the states*, 3rd ed.; Gale Research Company: Detroit, 1985.

(15) NREL. Renewable Resource Data Center. Wind Energy Resource Atlas of the United States: Chapter 3 Regional Summaries. The Southwest Region; 1983; available at http://rredc.nrel.gov/wind/pubs/atlas/chp3.html#southwest.

(16) Smith, D.R., Wind Farms of the Altamont Pass Area. *Ann. Rev. Energy* **1987** 12, 145-83.

(17) AWS Truewind. *Draft Boundary Layer Research and Findings Report*. **2005**; available at http://energy.ca.gov/2006publications/CEC-500-2006-062/CEC-500-2006-062-AP4.PDF.

(18) Lawrence Livermore National Laboratory. Wind Farm Maps for Altamont Pass, San Gorgonio Pass, and Tehachapi Pass; 2007; available at https://eed.llnl.gov/renewable/maps/.

(19) Mesinger, F. et al. North American Regional Reanalysis, *Bull. Amer. Meteor. Soc.* **2006** 87, 1-42.

(20) UCAR. Overview of NCL; 2009; available at http://ncl.ucar.edu/overview.shtml.

(21) Atkinson, B.W., *Dynamical Meteorology: An Introductory Selection*; Methuen Young Books: London, U.K., 1981.

(22) Bouttier, F.; Courtier, P. Data assimilation concepts and methods, *ECMWF lecture notes* **1999**, 5.

(23) Earth Systems Research Laboratory. NCEP North American Regional Reanalysis: NARR Pressure level; 2009; available at http://cdc.noaa.gov/data/gridded/data.narr.pressure.html.

(24) Marshall, J. and Plumb, R. A. *Atmosphere, Ocean, and Climate Dynamics, Volume 93: An Introductory Text*; Academic Press: Boston, 2008.

(25) USGS National Map Viewer. United States Geological Survey; 2009; available at Last http://nmviewogc.cr.usgs.gov/view.htm.

(26) Pasquill, F. The estimation of the dispersion of windborne material. *The Meteorological Magazine* **1961** 90 (1063), 33-49.

(27) Nelson, V. *Wind Energy: Renewable Energy and the Environment*; CRC Publishing: Kansas City, 2009.

(28) Elliot, D.L. Adjustment and analysis of data for regional wind energy assessments. Workshop on Wind Climate, Asheville, NC, November 12-13, 1979.

(29) Golder, D. Relations among stability parameters in the surface layer. *Boundary Layer Meteorology* **1972**, 3, 47-58.

(30) Stull, R. B. *An Introduction to Boundary Layer Meteorology*; Kluwer Academic Publishers: Boston, 1988.

(31) Paulson, C. A. The mathematical representation of wind speed and temperature in the unstable atmospheric surface layer. *J. Appl. Meteor.* **1970** 9, 857-861.

(32) Businger, J.A.; Wyngaard, J.C.; Izumi, Y.; Bradley, E.F. Flux profile relationships in the atmospheric surface layer, *J. Atmos. Sci.* **1971**, 28, 181-189.

(33) Dyer, A.J. A review of flux-profile relations, *Boundary-Layer Meteorology* **1974**, 7, 363-372.

(34) NREL. Renewable Resource Data Center. Wind Energy Resource Atlas of the United States: Appendix A. Wind Power Classes; 1983; available at http://rredc.nrel.gov/wind/pubs/atlas/appendix_A.html#wind.

(35) Peterson, E.W.; Hennessey Jr., J. P. On the use of power laws for estimates of wind power potential, *J. Appl. Meteorology*, **1978** 17, 390-394.

(36) NREL. Renewable Resource Data Center. Wind Energy Resource Atlas of the United States: Appendix D. Comparison of Actual and Extrapolated Power at 50m; 1983; available at http://rredc.nrel.gov/wind/pubs/atlas/appendix_D.html#power.

(37) Golden Gate Weather Services. El Nino Years and Intensities; 2009; available at http://ggweather.com/enso.oni.htm.

(38) Unidata. NetCDF FAQ: What Is netCDF?; 2009; available at http://
unidata.ucar.edu/software/netcdf/docs/faq.html#whatisit.

(39) Earth System Grid II. Overview: Turning Climate Model Datasets into Community
Resources; 2002; available at http://earthsystemgrid.org/about/overviewPage.do.

(40) Nakicenvoic et al. *Special Report on Emissions Scenarios. A Special Report of Working Group III of the Intergovernmental Panel on Climate Change*; Cambridge University Press: Cambridge U.K., 2000.

(41) Scripps Institute of Oceanography and NOAA/ESRL. Mauna Loa CO2 Monthly Mean
Data; 2009; available at ftp://ftp.cmdl.noaa.gov/ccg/co2/trends/co2_mm_mlo.txt.

(42) GRID-Arendal. IPCC Special Report on Emissions Scenarios: Chapter 4, an Overview
of Scenarios: A2 Storyline and Scenario Family; 2009; available at http://
grida.no/publications/other/ipcc_sr/?src=/climate/ipcc/emission/094.htm.

(43) Rahmstorf, S. A semi-empirical approach to projecting future sea-level rise. *Science* **2007**
315 (5810), 368-370.

(44) Canadian Centre for Climate Modelling and Analysis. The third generation coupled
global climate model (CGCM3); 2005;
 available at http://www.cccma.bc.ec.gc.ca/models/cgcm3.shtml.

(45) _____. CRCM4.2.3 time-slice simulation for 1961-2100: Cautionary Note; 2009;

 available at http:// cccma.ec.gc.ca/data/crcm423/crcm423_aet_sresa2.shtml.

(46) Pal, J. S., et al. Regional Climate Modeling for the Developing World: The ICTP

RegCM3 and RegCNET. *Bull. Amer. Meteor. Soc.* **2007** 88, 1395–1409.

(47) Delworth, T.L. et al., GFDL's CM2 Global Coupled Climate Models. Part I:

Formulation and Simulation Characteristics, *J. Climate* **2006**, 19, 643–674.

(48) Miller, et al., An Analysis of Simulated California Climate Using Multiple Dynamical and

Statistical Techniques. California Climate Change Center; 2009; available at

http://energy.ca.gov/2009publications/CEC-500-2009-017/CEC-500-2009-017-F.PDF.